# Preservation and degradation of ancient organic matter in mid-Miocene Antarctic permafrost

Marjolaine Verret<sup>1</sup>, Sebastian Naeher<sup>2,3</sup>, Denis Lacelle<sup>4</sup>, Catherine Ginnane<sup>3</sup>, Warren Dickinson<sup>5</sup>, Kevin Norton<sup>2</sup>, Jocelyn Turnbull<sup>3,6</sup>, Richard Levy<sup>3,5</sup>

Department of Arctic Geology, The University Centre in Svalbard, Longyearbyen, 9170, Svalbard and Jan Mayen.
School of Geography, Environment and Earth Sciences, Victoria University of Wellington, Wellington, 6011, New Zealand.
GNS Science, Lower Hutt, 5010, New Zealand.

<sup>4</sup>Department of Geography, Environment and Geomatics, University of Ottawa, Ottawa, K1N 6N5, Canada.

<sup>5</sup>Antarctic Research Centre, Victoria University of Wellington, Wellington, 6011, New Zealand.

<sup>6</sup>CIRES, University of Colorado at Boulder, USA.

Correspondence to: Marjolaine Verret (marjolainv@unis.no)

the McMurdo Dry Valleys under the current warming climate.

Abstract. The Antarctic environment is amongst the coldest and driest environments on Earth. The ultraxerous soils in the McMurdo Dry Valleys support exclusively microbial communities, however, 15 million years ago, a tundra ecosystem analogous to present-day southern Greenland occupied this region. The occurrence of ancient soil organic carbon combined with low accumulation of contemporary material makes it challenging to differentiate between ancient and modern organic processes. Here, we explore the additions of modern organic carbon, and the preservation and degradation of organics and lipid biomarkers, in a 1.4 m mid-Miocene age (~14.5-14.3 Ma) permafrost soil column from Friis Hills. The total organic carbon is low throughout the soils (< 1%wt). The near-surface (upper 35 cm) dry permafrost has lower C:N ratios, higher  $\delta^{13}$ Corg values, higher proportion of branched fatty acids with an iso- and anteiso- configuration relative to *n*-fatty acids, lower phytol abundance and higher contributions of low-molecular weight homologues of n-alkanes, than the underlying icy permafrost, indicating higher contributions from bacteria-derived organic matter. Conversely, the icy permafrost contains higher molecular weight n-alkanes, n-fatty acids and n-alkanols, along with phytosterols (e.g., sitosterol, stigmasterol) and phytol (and its derivatives pristane and phytane) that are indicative of the contributions and preservation of higher-level plants. This implies that legacy mid-Miocene age carbon in the near-surface soils (c. 35 cm) has been prone to microbial organic matter degradation during times when the permafrost thawed, likely during relatively warm intervals through the late Neogene (~6.0 Ma) and sporadically during the Holocene (<1%), when ground summer temperatures were ≥+2°C (based on brGDGTs temperature reconstructions). Conversely, Jipid biomarkers, found deeper in the permafrost have been preserved for millions

#### 30 1 Introduction

The McMurdo Dry Valleys (MDV) are amongst the coldest and driest environments on Earth (e.g. Horowitz et al., 1972). This, hyperarid polar desert can be divided into three microclimate zones (Marchant and Head III, 2007): (i) the coastal thaw (or

of years. These results suggest that ancient organics preserved in permafrost could underpin significant ecological changes in

Deleted: input rates

Deleted: more recent

Deleted: document

**Deleted:** iso-FAs relative to *n*-FAs

Formatted: Font: Italic

Deleted: marginally

Deleted: through

Deleted: a

Deleted: L

Deleted: Biomolecules

Deleted: se

**Deleted:** as Earth's current climate warms in the coming decades and centuries

Deleted: e

1

subxerous) zone (<400 m above sea level; a.s.l.) where mean daily summer air temperatures exceed 0°C and soil water can exist seasonally; (ii) the inland mixed (or *xerous*) zone where summer air temperatures may rise above 0°C for short periods and where soil water may be present periodically; and the *ultraxerous* or stable upland zone, where maximum air temperatures rarely exceed 0°C and snow is scarce (<10 mm water equivalent per year). The MDV lack vascular plants, and the subxerous zone contains edaphic communities with sparse cryptogamic vegetation (mosses and lichens), low diversity of invertebrates, and heterotrophic soil organisms, as well as endolithic communities of phototrophic and heterotrophic organisms in sandstone outcrops and other lithic substrates (e.g. Bargagli et al., 1999; Barrett et al., 2007; Cary et al., 2010; Freckman and Virginia, 1997; Horowitz et al., 1972; Moorhead et al., 2002). By contrast, the ultraxerous zone lacks all types of edaphic vegetation and appears to only support endolithic organisms in sandstone outcrops (Friedmann, 1982). Heterotrophic microbial communities are present in soils but at very low metabolic levels or in a dormant state (Goordial et al., 2016; Tamppari et al., 2012). Similar conclusions were drawn from the Shackleton Glacier region, a region situated further inland in the Transantarctic Mountains, where cultivation-dependent, cultivation-independent and metabolic assays were unable to detect viable microbial life (Dragone et al., 2021). However, in places in University Valley (Fig. 1a) where the ground surface raises above 0°C in summer, the permafrost contains about 5× more organic carbon ( $C_{org}$ ), and microbial activity has been indirectly inferred from C:N ratios,  $\delta^{13}C_{org}$  and  $\delta^{13}C_{caCO3}$  (Faucher et al., 2017).

The studies about the source and cycling of Corg in University Valley were from permafrost cores that represents about 152 kyr of sediment accumulation (Lacelle et al., 2013). At Friis Hills (Fig. 1a), the permafrost consists of early to middle Miocene age sediments (Chorley et al., 2023; Lewis and Ashworth, 2016), and is potentially the oldest permafrost on Earth (Verret et al., 2021). During the mid-Miocene (~20-14.6 Ma), the region harboured a tundra environment (Lewis and Ashworth, 2016; Chorley et al., 2023; Lewis et al., 2008) analogous to that found in southern Greenland today (including vascular plants). Since there have been limited periods of melt since the mid-Miocene (Verret et al., 2023), the site offers the opportunity to analyse the preservation and degradation of organic carbon in permafrost over millions of years. Lipid biomarkers are among the most stable organic molecules and can be preserved over long time periods (e.g. Naeher et al., 2022; Schouten et al., 2013; Castañeda and Schouten, 2011; Duncan et al., 2019). Low-molecular weight organic compounds (e.g. sugars and amino acids) and lipids with double bonds or polar functional groups (e.g. fatty acids and alcohols) are typically susceptible to microbial decomposition. However, other lipid biomarkers, such as apolar, saturated hydrocarbons (e.g. alkanes), isoprenoids (e.g. phytane) and cyclic compounds (i.e. hopanes or steranes), are refractory compounds formed during diagenesis (Peters et al., 2004b) and may be preserved on geological timescales (e.g. Eigenbrode, 2008). Over large timescales, both biotic and abiotic degradation occurred at Friis Hills. Abiotic degradation would result in the organic material near the surface to be better preserved (due to the principle of superposition). However, in a permafrost environment, biotic degradation, which is restricted to the active layer (layer that thaws in freezes on an annual basis), would overprint the abiotic degradation and would be more important near the surface: incorporating both contemporary and ancient organic carbon into the system (Kusch et al., 2021), As such, the distribution and occurrence of biomarkers in the Friis Hills Miocene age sediments can provide insight about Deleted: of

Deleted: for long

Deleted: which

**Deleted:** during warmer climate intervals

Deleted: (Kusch et al., 2019)

Deleted: ir

Formatted: Font color: Auto, English (CAN)

depositional conditions as well as paleoenvironmental changes post deposition (e.g. Duncan et al., 2019)

In this study, we investigate the source of ancient carbon reservoirs, degradation and potential overprint of modern organic carbon sources by combining bulk organic carbon and nitrogen analyses (TOC, total N,  $\delta^{13}C_{erg}$ ), with lipid biomarker indicators, ramped pyrolysis-gas chromatography-mass spectrometry (Py-GC-MS), and radiocarbon dating. We also use bacterial branched glycerol dialkyl glycerol tetraether (brGDGT) lipids to infer threshold temperatures required to unlock organic carbon stored within the permafrost. The exposure of ancient organic carbon to modern degradation at Friis Hills provides valuable information on the present-day organic processes, which can be juxtaposed to the distinct organic signature of the tundra environment that dominated the site during sediment deposition. This allows us to assess the degradation of ancient organic carbon pools, soil carbon mineralization and cycling in the context of a warming Antarctic climate.

5 2 Study Site

The Friis Hills (77°45'S, 161°30'E, 1200-1500 m a.s.l.) are a 12 km wide inselberg situated at the head of Taylor Valley, ca. 50 km from the Ross Sea coast (Fig. 1a). The Friis Hills are situated within the ultraxerous zone (Marchant and Head III, 2007), where modern climatic conditions are extremely cold and arid, and microbial life is limited. The mean annual air temperature is -22°C, with an average reaching -13°C during the summer months (Friis Hills Meteorological Station 2011-2015; Doran and Fountain, 2016). The area receives less than 10 mm snow water equivalent of precipitation per year, most of which is displaced by strong katabatic winds (yearly average wind speed at Friis Hills is 4.7 m s<sup>-1</sup>; Bliss et al., 2011). The local geology consists primarily of Ordovician and Jurassic age intrusive igneous rocks and Devonian sedimentary rocks of the Beacon Supergroup (Allibone et al., 1993; Lewis and Ashworth, 2016; Cox et al., 2012). A ca. 80 m thick sequence of glacial drifts interbedded with lacustrine sediments record multiple episodes of advance and retreat of local alpine glaciers and intervals of ice sheet over-riding (Chorley et al., 2023; Lewis and Ashworth, 2016).

Deleted: diagenetic

Deleted: i

Deleted: total Corg

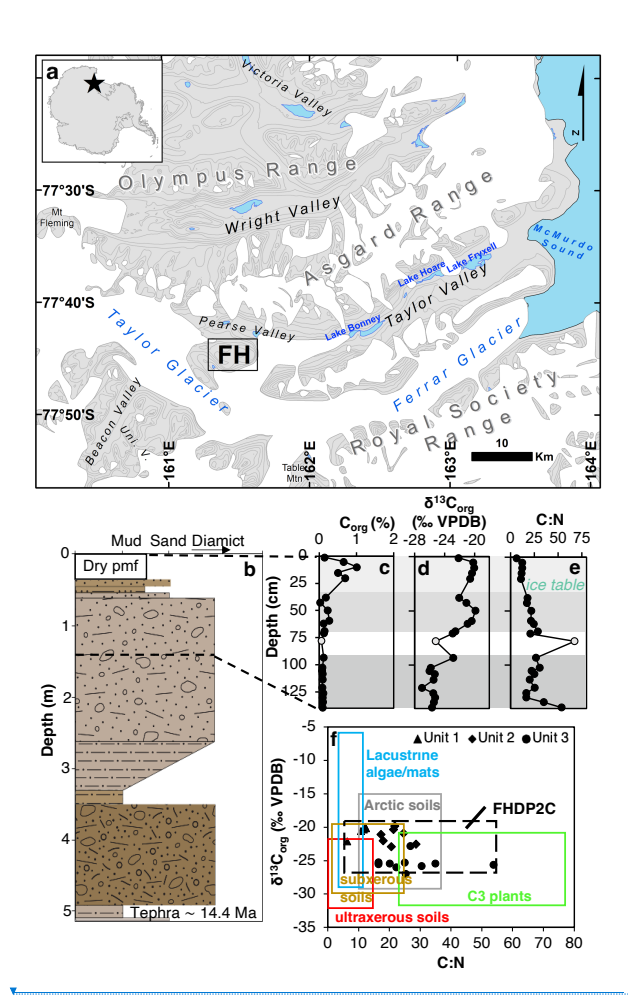
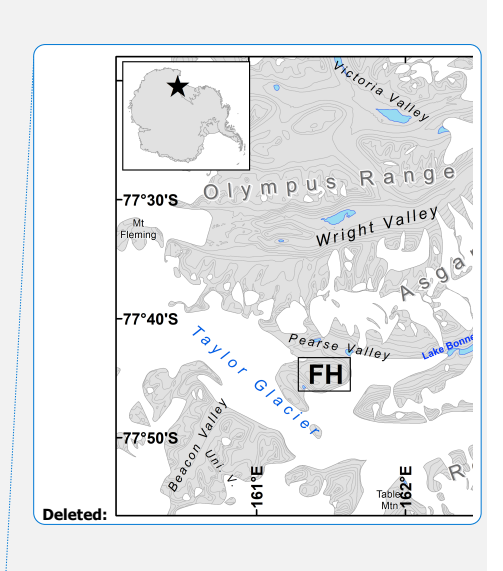


Figure 1 a. Location map of Friis Hills (FH) within the McMurdo Dry Valleys of Antarctica. Contour lines at 200 m intervals. by sedimentary log of core FHDP2C from Friis Hills with the upper 140 cm studied in detail in this paper, where colours reflect Munsell colours of each unit. c. organic carbon concentration, expressed in wt%, d.  $\delta^{13}$ C, e. C.N ratio and f.  $\delta^{13}$ Corg and C:N biplot with bulk sediment measurements from three different units in FHDP2C compared to ultraxerous environments: University Valley and Mackay Glacier (Faucher et al., 2017; Van Goethem et al., 2020), subxerous environments; Miers, Garwood, Taylor and Victoria Valleys (Barrett et al., 2007; Hopkins et al., 2009). Antarctic lake/stream mats (Hopkins et al., 2009; Lawson et al., 2004). Arctic soils (Haugk et al., 2022; Osburn et al., 2019) and signature for C3 plants (Meyers, 1994). Unit separation was established by hierarchical clustering.



Deleted: B

**Deleted:** Uncovered ice table at Friis Hills, overlain by a 35 cm thick layer of dry permafrost (photo credit: H. Chorley).

Major paleoenvironmental changes at Friis Hills can be divided into four distinct periods: (1) the early to mid-Miocene, a period when tundra persisted in the Friis Hills and throughout many locations across the Transantarctic Mountains (~20–14.6 Ma; Lewis et al., 2008; Duncan et al., 2019), (2) a period when tundra vegetation disappeared from high elevation localities in the MDV (~13.8 to 12.5 Ma; Lewis et al., 2008; Lewis and Ashworth, 2016; Chorley et al., 2023); (3) the mid-late Miocene (12.5–6.0 Ma), a period through which high elevations became progressively drier, culminating in hyper-arid conditions (Verret et al., 2023); and (4) the late Neogene and Quaternary (6.0 Ma–present) period, when the high elevations remained frozen and hyper-arid, even during relatively warm interglacial conditions. Low erosion rates (on the order of 0.1 m Myr<sup>-1</sup>) associated with a relatively cold and dry environment enhanced the preservation of the sediment record through the Neogene, while exposing the mid-Miocene organic carbon to surficial processes (Verret et al., 2023).

The Friis Hills Drilling Project (FHDP) recovered a series of sediment cores from three sites (1, 2, and 3) during the 2016-17 Antarctic Field season (Chorley et al., 2023). Three cores (A, B, and C) were drilled at Site 2 (77°45'17.028''S,

135 161°27′20.632″E, 1244 m a.s.l.) and this study focuses on the uppermost 140 cm of the ~5 m<sub>F</sub>long core 'C' (FHDP2C; Fig. 1a). The ice table (i.e. the boundary between the dry and the ice-cemented permafrost) occurs at 35 cm below the top of the core (Figs. 1b & S1). The detailed age model of the FHDP cores is presented in Chorley et al. (2023). The lower section of core FHDP2C, which directly correlates with core FHDP2A, is constrained by <sup>40</sup>Ar/<sup>39</sup>Ar dating of a tephra at 5.13-5.18 m depth (14.4 Ma; Fig 1b). The most parsimonious solution for the normal chronology above the ash is that it is C5AD (~14.6 to 14.2
 140 Ma), corresponding to the mid-Miocene climate transition (MMCT; Flower and Kennett, 1994; Shevenell et al., 2004).

Furthermore, the analyzed sediments are from the upper part of sequence 13 from the Friis Hills composite presented in (Chorley et al., 2023). This sequence was likely deposited during a single precession cycle between 14.36 and 14.38 Ma (see Fig. 11 in Chorley et al., 2023) although we acknowledge that it may have been deposited during alternate precession cycles between ~14.4 and 14.2 Ma. Independent cosmogenic surface exposure dating at Friis Hills also suggests a minimum age of the surface of 11 Ma (Valletta et al., 2015).

The FHDP2C core includes two sedimentary cycles comprising two glacial (i.e., matrix-supported diamicts attributed to subglacial traction tills) and two interglacial facies (i.e., muddy-sand units attributed to proglacial ponds). An assemblage of organic macrofragments such as lichens, liverworts, mosses, dicots, grasses and sedges, along with cuticles belonging to the *Nothofagaceae* family were observed within core samples (Chorley et al., 2023). Similar plant assemblages are widespread in the modern southern Greenland or Svalbard in the Arctic (e.g. Berke et al., 2019). Tundra macrofossils are found in all sedimentary facies but are most prevalent in the finer grained units, suggesting that higher plants were relatively abundant across the Friis Hills during the interglacial periods. These data indicate that the mid-Miocene climate at relatively high elevations in the MDV region of the Transantarctic Mountains remained warm and wet enough to support growth of higher plants (Chorley et al., 2023), after which tundra vegetation disappeared from these elevations (Lewis et al., 2008).

150

Deleted:

Deleted: etre

Deleted: 2

Deleted:

**Deleted:** Magnetostratigraphy constrained by <sup>40</sup>Ar/<sup>59</sup>Ar dating of a tephra at 5.13-5.18 m depth indicate the sedimentary sequence in FHDP2C was deposited between ~14.5 and ~14.5 Ma (magnetozone 1N1, C5Acn; 14.070 to 13.739 Ma; Chorley et al., 2023)

Deleted:

### 3 Methods

### 3.1 Core description and sampling

Lithological descriptions were undertaken in the field and cross-checked on the frozen core prior to sampling at GNS Science's National Ice Core Facility, Lower Hutt, New Zealand. The core was sub-sampled at ~5 cm intervals using a tile cutter with a 2.2 mm thick blade and samples were placed into polyethylene bags to thaw before being dried at 80°C for 24 hours (plastic contamination was not found in the samples). The surficial dry permafrost layer was sampled in the field at 5 cm intervals. A total of 23 samples from the upper 140 cm of the core were analysed for bulk organic carbon and nitrogen and lipid biomarkers.

# 3.2 Bulk carbon and nitrogen analysis

and ii) if the C:N ratios in the bulk sediments follow the Redfield biological stoichiometry ratio (6:61; Redfield, 1934). The TOC and TN was measured using an Elemental VarioEl Cube instrument at the Jan Veizer Laboratory, University of Ottawa, Canada. The samples were first acidified with 10% HCl to remove the inorganic carbon and isolate the organic carbon fraction. 100 mg of sediment was analysed within tin capsules, along with 100 mg of tungstic oxide (WO<sub>3</sub>), a combustion catalyst and binder. Calibrated standards of Sulfanilic Acid were prepared in a range of weights and ran cyclically to ensure instrument precision, and approximately 20% of samples were analysed in duplicate with analytical precision of ± 0.1%.

The total organic carbon (TOC) and total nitrogen (TN) were measured to determine: i) the soil organic carbon density (SOCd),

The  $\delta^{13}C_{org}$  of the bulk samples was measured using a DeltaPlus Advantage instrument coupled with the ConFlo III interface to assess potential source and alteration of organic carbon in the sediments. The results are expressed in  $\delta$  notation, which represents the parts per thousand difference of  $^{13}C/^{12}C$  in per mil (%) with respect to the Vienna Pee-Dee Belemnite (VPDB) standard. Analytical precision was  $\pm$  0.2%.

### 3.3 Lipid biomarker analyses

Lipid biomarkers were analysed to differentiate between the mid-Miocene tundra carbon and subsequent microbial degradation. Lipid biomarkers were analysed in the Organic Geochemistry Laboratory at GNS Science, Lower Hutt, New Zealand, following Naeher et al. (2012; 2014) with some modifications. Homogenised sediment (~5–15g) was extracted 4× by ultrasonic extraction using dichloromethane (DCM):methanol (MeOH) (3:1, v:v). Total lipid extracts (TLEs) were saponified using 6% KOH in MeOH at 80°C for 3 hours. After the addition of ultrapure H<sub>2</sub>O, neutrals were extracted from the aquatic solution using *n*-hexane. Following acidification with 6M HCl to pH <2, fatty acids (FAs) were then 190 recovered using *n*-hexane.

The neutral fraction was further separated into apolar and polar fractions by silica gel chromatography using *n*-hexane and DCM:MeOH (1:1, v: v), respectively. Prior to analysis by gas chromatography-mass spectrometry (GC-MS), an aliquot of the polar fraction, was, derivatized with BSTFA in pyridine at 80°C for 1 hour, whereas FA fractions were derivatized with BF<sub>3</sub> MeOH at 100°C for 2 hours to obtain fatty acid methyl esters (FAMEs).

Deleted: ,	
Deleted: as	
Deleted:	

Deleted: s

Deleted: ere

200 The resulting lipid fractions were analysed by GC-MS on an Agilent 7890A GC System, equipped with an Agilent J&W DB-5ms capillary column [60 m × 0.25 mm inner diameter (i.d.) × 0.25 μm film thickness (f.t.)], and coupled to an Agilent 5975C inert MSD mass spectrometer. The oven was heated from 70°C (held for 1 min) to 100°C at 20°C min<sup>-1</sup>, then to 320°C at 4°C min<sup>-1</sup> and held at that temperature for 20 minutes. Helium was used as carrier gas with a constant flow of 1.0 ml min<sup>-1</sup>. Samples (1 μl) were injected splitless at an inlet temperature of 300°C. The MS was operated in electron impact ionisation mode at 70 eV using a source temperature of 230°C.

Lipid biomarkers were quantified relative to an internal standard (50  $\mu$ L added to the TLEs following solvent extraction; consisting of 110.8  $\mu$ g ml<sup>-1</sup> 5 $\alpha$ -cholestane, 118.8  $\mu$ g ml<sup>-1</sup> n-nonadecanoic acid and 116.8  $\mu$ g ml<sup>-1</sup> n-nonadecanol). Procedural blanks were also analysed to ensure data quality and absence of laboratory contamination.

Another aliquot of the polar fraction, containing glycerol dialkyl glycerol tetraethers (GDGTs) were dissolved in *n*-hexane/isopropanol (99:1, v:v) and filtered with 0.45 μm PTFE filters prior to analysis by high performance liquid chromatography-atmospheric pressure chemical ionisation-mass spectrometry (HPLC-APCI-MS) as reported in Hopmans et al. (2016). These analyses were undertaken on an Agilent 1260 Infinity II Prime LC system coupled to an Agilent 6125B single quadrupole MS following the method of Hopmans et al. (2016). In brief, two UHPLC silica columns (Acquity BEH HILIC columns, 2.1 × 150 mm, 1.7 μm; Waters) were used in series, fitted with a 2.1 × 5 mm pre-column of the same material (Waters), and maintained at 30°C. GDGTs were eluted isocratically for 25 minutes with 82% A:18% B, followed by a linear gradient up to 35% B in 25 minutes, then a linear gradient to 100% B in 30 min, where A is *n*-hexane and B is *n*-hexane/isopropanol (9:1, v/v). Flow rate was 0.2 ml/min. The abundances of GDGTs were monitored using selective ion monitoring mode (SIM) with *m/z* 1302, 1300, 1298, 1296, 1294, 1292, 1050, 1048, 1046, 1036, 1034, 1032, 1022, 1020, 1018. Compounds were identified by comparing mass spectra and retention times with those in the literature (e.g. Hopmans et al., 2016). The concentration of biomarkers is expressed in microgram per gram of TOC (μg g<sup>-1</sup> TOC).

3.4 Lipid biomarker proxies and indices

The <u>concentrations</u> of the lipid biomarkers were used to calculate a series of indices to: i) differentiate between plant- and bacteria-derived organic carbon; and ii) define the level of degradation of the organic carbon.

225 3.4.1 Carbon preference index

230

The carbon preference index (CPI) is a parameter that quantifies the ratio of odd to even *n*-alkanes and ratio of even to odd *p*-fatty acids based on its carbon number and is an indicator of the degradability of organic carbon. Natural distributions or well-preserved *n*-alkane signatures are expected to show a predominance of odd-numbered *p*-alkanes and even numbered *p*-fatty acids corresponding to high CPI values. The CPI value decreases with ongoing alteration of organic carbon (Bray and Evans, 1961):

Deleted: T

Deleted: s

**Deleted:** measurements

Formatted: Font: Italic

Moved (insertion) [2]

Formatted: Font: Italic

Formatted: Font: Italic

**Deleted:** carbon chains because of decarboxylation of fatty acids that show characteristic even carbon number predominance

$$CPI_{25-33} = 0.5 \cdot \left( \frac{\sum odd \, C_{25-31}}{\sum even \, C_{26-32}} + \frac{\sum odd \, C_{27-33}}{\sum even \, C_{26-32}} \right) \tag{1}$$

A similar index was also calculated for fatty acids and n-alcohols (Meyers and Ishiwatari, 1993):

$$CPI_{22-28} = \frac{\sum even c_{22-26} + \sum even c_{24-28}}{2 \cdot \sum odd c_{23-27}}$$
 (2)

### 3.4.2 Average chain length and dominant chain length

In general, cuticle waxes of terrestrial plants contain predominantly high-molecular weight n-alkanes (>n-C<sub>27</sub>; with leaf waxes containing mainly n-C<sub>27</sub> and n-C<sub>29</sub> and grasses containing mainly n-C<sub>31</sub> and n-C<sub>33</sub> alkanes) while mid molecular weight (n-C<sub>21</sub> to n-C25) alkanes are indicative of aquatic macrophytes, mosses (e.g. Sphagnum in peat) or lichen, and low-molecular weight (n-C<sub>12</sub> to n-C<sub>20</sub>) alkanes are common in algae and bacteria (e.g. Naafs et al., 2019; Killops and Killops, 2013; Zech et al., 2010). A similar relation can be extracted from even carbon numbered n-alkanols and n-fatty acids. The average chain length 245 (ACL) of n-alkanes can be used to identify the main source of organic carbon and it can be useful to infer environmental changes in a particular ecosystem (e.g. Killops and Killops, 2013). The ACL was calculated for odd-chain n-alkanes with C27 to C<sub>33</sub> following this equation (Poynter and Eglinton, 1990):

$$ACL_{C27-C33} = \frac{\sum_{i} c_{i}}{\sum_{i} c_{i}}$$

$$\tag{3}$$

where i is the carbon number and  $C_i$  is the concentration of n-alkane.

ACL was also calculated for even-chain FAME (C22 to C32) and n-alkanols (C22 to C28). We also present the dominant chain length (C<sub>max</sub>) for each biomarker class.

### 3.4.3 Ratio of short-chain and long-chain n-alkanes

The ratio of short-chain n-alkanes (SC,  $< C_{23}$ ) and long-chain n-alkanes (LC,  $\ge C_{23}$ ) was calculated using the following equation:

255 
$$SC:LC = \frac{\sum C_{C15-C22}}{\sum C_{C23-C33}}$$
 (4)

High values of SC:LC are indicative of an environment dominated by bacteria while low values are indicative of an environment dominated by higher plants and/or macrophyte waxes (e.g. Killops and Killops, 2013).

# 3.4.4. Other indices derived from saturated hydrocarbons, isoprenoids and fatty acids,

260 The ratio of iso- and anteiso-FA to p-FA was calculated for the chain lengths detected in the samples  $(C_{45}-C_{47})$  and expressed with a ×100 factor for ease of comparison. Branched FA compounds are diagnostic indicators of bacteria (e.g. Kaneda, 1991).

The pristane to phytane ratio (Pr:Ph) is used as a redox indicator (Powell, 1988; Naeher and Grice, 2015) and higher values reflect oxygenated conditions, which may represent increased anaerobic microbial degradation.

Moved up [2]: Natural distributions or well-preserved n-alkane signatures are expected to show a predominance of odd-numbered carbon chains because of decarboxylation of fatty acids that show characteristic even carbon number predominance

Deleted: This typically reflects the degree of bacterial alteration during diagenesis, as odd chains get altered into smaller chain lengths, while their odd-over-even predominance decreases (Bray and Evans, 1961; Grimalt et al., 1985).

### Deleted:

Deleted:

Formatted: Font: Italic Formatted: Font: Italic

#### Deleted: 3.4.4 Higher plant fatty acid index

The higher plant fatty acid index (HPFA), which can be used as a relative indicator of chemical degradation, was calculated following this equation (Strauss et al., 2015): ¶ HPFA =

 $\sum fatty\ acids\ C_{24}$ , $C_{26}$ , $C_{28}$ 

 $\sum fatty\ acids\ c_{24}.c_{26}.c_{28} + \sum n-alkanes\ c_{27}.c_{29}.c_{31}$ Since *n*-alkanes are typically preserved better than *n*-fatty acids, low HPFA are indicative of high degrees of organic carbon degradation.

Formatted: Font: Bold

Formatted: Font: Bold Formatted: Font: Bold

Formatted: Font: Bold Formatted: Font: Italic

Formatted: Subscript

Formatted: Subscript

Since the natural  $\beta\beta$  isomer in  $C_{\delta0}$  hopane is mostly present in modern organic material, we use the  $C_{\delta0}$   $\alpha\beta/(\alpha\beta+\beta\alpha+\beta\beta)$ Formatted: Subscript Formatted: Subscript hopane index to infer the relative input of new bacterial-derived organic material (with a ratio <0.5 representing input 285 of recent organic matter; Peters et al., 2004a; Farrimond et al., 1998). 3.4.5, brGDGT indices Deleted: 5 The branched and isoprenoid tetraether (BIT) index, which differentiates between inputs from a terrestrial environment (BIT Deleted: h  $\approx$  1) and a marine environment (BIT  $\approx$  0) was calculated as follows (Hopmans et al., 2004): Deleted: BIT Index =  $\frac{(I+II+III)}{(I+II+III+IV)}$ Deleted: (7) where I, II and III denote the relative abundances of brGDGTs and IV reflects the relative abundance of crenarchaeol. Past summer soil temperatures (Raberg et al., 2024) were estimated using the MBT'<sub>5ME</sub> index (De Jonge et al., 2014) and the soil-specific, Bayesian temperature calibration BayMBT<sub>0</sub> of Crampton-Flood et al. (2020). The MBT'<sub>5ME</sub> index was calculated  $MBT'_{5ME} = \frac{III_a + II_a + II_b + II_c + I_a + I_b + I_c}{III_a + II_a + II_b + II_c + I_a + I_b + I_c}$ (8) 295 3.6 Radiocarbon and Pyrolysis-GC-MS analysis Deleted: 5 To determine if biogeochemical processes are relict or currently active at Friis Hills, one sample of dry sediment (2-C0-3; 10 Moved (insertion) [3] cm depth) was measured for radiocarbon content at the Rafter Radiocarbon Laboratory, GNS Science. The bulk sediment Deleted: activity sample (< 300 µm) was first acid-treated to remove carbonates and then combusted at 900°C for 4 hours in an evacuated. sealed quartz tube with cupric oxide and silver wire. The resulting CO<sub>2</sub> was graphitized by reduction with hydrogen over iron 300 catalyst and measured by accelerator mass spectrometry (Turnbull et al., 2015; Zondervan et al., 2015). Radiocarbon activity **Field Code Changed** is presented as F14C fraction modern carbon; Donahue et al., 1990; Reimer et al., 2004) and conventional radiocarbon age (as Field Code Changed described in Stuiver and Polach, 1977). To differentiate between ancient carbon reservoirs, diagenetic degradation and potential overprint of modern organic carbon 305 sources, ~2 g of dried, homogenized decalcified material from the same sample 2-C0-3 was prepared for thermochemicallypartitioned radiocarbon analysis using ramped pyrolysis oxidation-accelerator mass spectrometry (RPO-AMS) radiocarbon dating as reported in Ginnane et al. (2024). In brief, the sediment sample was apportioned into CO2 fractions according to Formatted: Subscript thermochemical lability. CO<sub>2</sub> was evolved from sample 2-CO-3 by pyrolysis with a constant ramp of 5°C min<sup>-1</sup> from room Formatted: Subscript temperature to 750°C and subsequent oxidation, with discrete fractions collected from 105°C at 259, 395, 449, 535 and 750°C, Formatted: Superscript respectively. The obtained CO2 for each split was recombusted at 500°C with cupric oxide and silver wire and then graphitised Formatted: Subscript and measured in the same way as the bulk sediment. The same sample was also analysed by full, rapid-ramp pyrolysis and then incremental, partitioned ramped Py-GC-MS analysis Deleted: 1 in the Organic Geochemistry Laboratory at GNS Science to characterize the composition and sources of the organic carbon at Deleted: in the dry permafrost (sample 2-C0-3) was

different temperatures (Ginnane et al., 2024). For this, 37-50 mg of the sample was pyrolyzed in deactivated stainless-steel

cups. For full, rapid-ramp pyrolysis, samples were pyrolyzed with a ramp of 100°C min<sup>-1</sup> from 100°C to the Py-GC-MS instrumental maximum of 650°C. For incremental, partitioned ramped-Py-GC-MS, sample splits were obtained similar to RPO-AMS analysis by utilizing thermal desorption mode with a ramp of 10°C min<sup>-1</sup> run from 100°C to 259°C as the first split, then the subsequent splits collected to their respective maximum temperatures (395, 449, 535 and 650°C). After each split collection, the sample was removed from the pyrolyser furnace and GC-MS analysis of this step was completed, before reinserting the same sample cup and heating to the next split maximum temperature. The front inlet of the GC over was set to 5:1 split and the GC oven programme started at 40°C (held 5 min isothermal), ramped to 300°C at 5 °C min<sup>-1</sup>, and then held isothermal for 5 min. All other GC-MS settings were the same as described in Section 3.3.

Compounds were identified from the Py-GC-MS and grouped into nine compound classes following existing literature interpretations of dominant organic matter sources (i.e. bacteria or plant). The sources of *n*-alkanes were distinguished based on molecular weight (as detailed in section 3.4.2.). Pyrroles, furans and phenols were attributed to a plant-derived organic matter, as they are derived from pigments such as chlorophylls and polysaccharides (e.g. Keely, 2006). Polycyclic aromatic hydrocarbons, thiophenes, alkylbenzenes and other aromatics are undifferentiable compounds.

### 3.7 Statistical analysis

To simplify the data, we carried out hierarchical clustering of all 25 variables in R Studio 1.3.1056 using the *chclust* function in the package *rioja* with the method *coniss* (Juggins, 2020).

### 4 Results

335

The hierarchal clustering analysis of all samples in the 1.4 m sediment core and their 25 variables, which included TOC, C:N ratio,  $\delta^{13}C_{org}$ , lipid abundance and main biomarker indices, grouped the samples by depth. Group 1 consists of the dry permafrost from 0 to 35 cm depth; group 2 consists of the icy permafrost from 38 to 71 cm; and group 3 was the icy permafrost from 93 to 140 cm (Fig. 1b). An outlier sample (classified in a separate group) was identified at 79 cm depth and not included in any unit. The results first describe the general trends found throughout the core, followed by the variables and indices that are statistically different between the units.

### 4.1 General biomarker trends

We identified the following components within the 1.4m core: n-alkanes (n-C<sub>15</sub> to n-C<sub>34</sub>), isoprenoids, hopanoids, n-fatty acids with (n-C<sub>12</sub> to n-C<sub>30</sub>), branched fatty acids with iso- and anteiso- (n-C<sub>13</sub> to n-C<sub>17</sub>) configurations, n-alkanols (n-C<sub>12</sub> to n-C<sub>28</sub>), ketones, and sterols (Fig. 2). The distributions of n-alkanes, fatty acids and n-alkanols were dominated by high-molecular weight homologues, with ACL<sub>27-33</sub> of n-alkanes, ACL<sub>22-32</sub> of n-fatty acids and ACL<sub>22-28</sub> of n-alkanols averaging 28.7± 0.5, 24.0 ± 0.3 and 23.3 ±0.4 respectively, and showed little variation in the core (Fig. 2c). We also identified plant sterols (i.e. C<sub>20</sub> sterols)

Deleted: OM

Deleted: OM

Moved up [3]: To determine if biogeochemical processes are active at Friis Hills, one sample of dry sediment (2-C0-3; 10 cm depth) was measured for radiocarbon activity at the Rafter Radiocarbon Laboratory, GNS Science. The bulk sediment sample (< 300 µm) was first acid-treated to remove carbonates and then combusted at 900°C for 4 hours in an evacuated, sealed quartz tube with cupric oxide and silver wire. The resulting CO<sub>2</sub> was graphitized by reduction with hydrogen over iron catalyst and measured by accelerator mass spectrometry (Tumbull et al., 2015; Zondervan et al., 2015). Radiocarbon activity is presented as F<sup>14</sup>C (fraction modern carbon; Donahue et al., 1990; Reimer et al., 2004) and conventional radiocarbon age (as described in Stuiver and Polach, 1977). Ginnane et al. (2024)

#### Deleted: 3.6 Radiocarbon Analysis

To determine if biogeochemical processes are relict or currently active at Friis Hills, one sample of dry sediment (2-C0-3; 10 cm depth) was measured for radiocarbon activity at the Rafter Radiocarbon Laboratory, GNS Science. The bulk sediment sample (< 300 µm) was first acid-treated to remove carbonates and then combusted at 900°C for 4 hours in an evacuated, sealed quartz tube with cupric oxide and silver wire. The resulting CO<sub>2</sub> was graphitized by reduction with hydrogen over iron catalyst and measured by accelerator mass spectrometry (Tumbull et al., 2015; Zondervan et al., 2015). Radiocarbon activity is presented as F<sup>14</sup>C (fraction modern carbon; Donahue et al., 1990; Reimer et al., 2004) and conventional radiocarbon age (as described in Stuiver and Polach, 1977). Ginnane et al. (2024)

Deleted: 7

Deleted:

Deleted: classified in any group

Deleted:

**Deleted:** An ANOVA within subjects and post hoc Tukey HSD tests were then conducted on the results to determine whether the means of each variable in the three units were statistically different.

**Deleted:** Lipid biomarkers that show little variations throughout the 1.4 m core include:

Formatted: Normal

Formatted: Font: Italic

Formatted: Font: Italic

Deleted: The

Deleted: ged

**Deleted:** s 3d, 4d & 5d

**Deleted:** The cholesterol to plant sterol ratio remained low throughout the core (avg. 2.4; Fig. 5c), which indicates a terrestrial setting

Formatted: Subscript

most abundant), pristane and phytane along with hopanoids (Fig. 3). The GDGT analysis showed that the distribution of all samples was dominated by brGDGTs. All samples had a BIT index of 1.0, and MBT'5<sub>ME</sub> index ranged between 0.24 and 0.48 (Supplementary Data). In general, the homogenous distribution of these biomarkers in the core are indicative of a terrestrial environment with higher plant components such as high molecular weight *n*-alkanes, *n*-fatty acids and *n*-alkanols and plant sterols...

### 4.2 Group 1: dry permafrost (0-35 cm)

The dry permafrost had the highest TOC and TN concentrations, averaging 6.0 ± 0.3 and 0.53 ± 0.22 mg g<sup>-1</sup> dry soil, respectively (Fig. 1c). The C:N ratio averaged of 10.6 ± 2.5, which is near the Redfield ratio and suggests balanced microbial growth (Fig. 1c). The S<sup>13</sup>C<sub>org</sub> values were highest in the core, ranging from -22.1 to -20.0 %VPDB (Fig. 1d). The sum of odd *n*-alkane concentrations (avg. 628.2 μg g<sup>-1</sup> TOC; Fig. 2a), even *n*-fatty acids concentrations (avg. 1.67 mg g<sup>-1</sup> TOC; Fig. 2b) and even *n*-alkanols concentrations (avg. 432.1 μg g<sup>-1</sup> TOC; Fig. 2c) were all lowest in Unit 1. Within Unit 1, the CPI<sub>25-33</sub> of *n*-alkanes ranged from 3.7 to 6.9 (avg. 5.5 ± 1.2; Fig. 2d) and the SC:LC ratio from 1.6 to 7.7 (Fig. 3b); both of which are the highest values found in the core. The highest CPI<sub>22-28</sub> of *n*-fatty acids were also found in Unit 1 (Fig. 2d), along with the ratio of 100\*C<sub>15-17</sub> iso-FA+anteiso-FA/n-FA (up to 12.6; Fig. 3c). The dominant n-alkane chain length was C<sub>18</sub> (Fig. 2d). Hopanoids, which were detected in all measured fractions (as hopanes, hopanols and hopanoic acids), where highest in Unit 1 (avg. 84.6 ± 65.3 μg g<sup>-1</sup> TOC; Fig. 3a). Phytosterols such as stigmasterol and sitosterol and their derivatives were identified in highest concentrations in Unit 1, with the exception of the surface sample (Fig. 3g). Pr-Ph ratios were also highest in Unit 1 (avg. 6.2 ± 1.4; Fig. 3e) and C<sub>30</sub> αβ/(αβ+βα+ββ) was <0.5 in unit 1 (Fig. 3d).

A sample taken at 10 cm below the surface was <sup>14</sup>C dated and analyzed to determine the thermally partitioned splits. The sample taken at 10 cm below the surface yielded a bulk radiocarbon age of  $41,749 \pm 1,736$   $^{14}$ C yrs BP (F<sup>14</sup>C of  $0.0055 \pm 1.00$  graph of  $1.005 \pm 1.00$  graph  $1.005 \pm 1.005$  graph 1.0050.0012; Table 1). The lowest temperature split (105 to 259°C) is composed primarily of small, mostly undiagnostic molecules 420 that are mainly degradation products from larger (macro-)molecules (e.g. alkylbenzenes and other aromatics; Ginnane et al., 2024). In contrast, furans, which are found mostly in the 259 to 395°C partition (split 2) and 395 to 449°C partition (split 3), are diagnostic source indicators which can originate from carbohydrates, such as cellulose associated with the decay of terrestrial plants (e.g. Kaal, 2019). Pyrroles that are most abundant in split 2 are typical products of labile tetrapyrrole pigments (e.g. chlorophylls and its transformation products), whereas those found in split 4 are rather derived from the decomposition 425 of plant lignin (Keely, 2006). The highest two temperature splits (splits 4 and 5 collected from 449 to 535°C and 535 to 750°C respectively) are comprised of compounds that are mostly derived from alteration of more complex macromolecules commonly associated with more relict carbon or from secondary thermal reactions during pyrolysis at higher temperatures (Ginnane et al., 2024). The resulting compounds derived in these fractions commonly consists of more stable, older material including kerogen, that is less accessible to bacterial degradation. Overall, the TOC-TN and biomarker indices suggest a higher level of 430 organic carbon degradation by microbes relative to the underlying icy permafrost.

Deleted: Overall, these biomarkers reflect the background composition of the tundra-dominated ecosystem of the site during the mid-Miocene as inferred from the macrofossils. \( \left( ... [1] \)

Deleted: s
Deleted: 2b
Deleted: 2d
Deleted: 2c
Deleted: 3
Deleted: 4
Deleted: a
Deleted: 5
Deleted: a
Deleted: 3
Deleted: b
Deleted: c
Deleted: 4
Deleted: b
Deleted: 4
Deleted: 3e
<b>Deleted:</b> The HPFA remained <1 throughout the whole core, ranging from 0.3 to 1.0 (Fig. 4f), but was generally lower in U( [2])
Deleted: 6a
Deleted: 6b
Deleted: /

Deleted: 6d

Deleted:

## 4.3 Groups 2 and 3: icy permafrost (38-140cm)

The TOC and TN in the icy permafrost, averaging 2.0 ± 0.1 and 0.11 ± 0.09 mg g<sup>-1</sup> dry soil, respectively, were statistically lower than in the dry permafrost. The C:N ratios (16.4 to 53.7) were well above the Redfield ratio (Fig. 1c) The large range of C:N values in the icy permafrost may also partly be attributed to the low concentrations of N nearing the limit of analytical detection. The δ<sup>13</sup>C<sub>org</sub> values showed a general decrease with depth: -21.4 ± 1.1 ‰VPDB in unit 2, and -25.4 ± 1.0 ‰VPDB in unit 3; (Fig. 1d). The sum of odd *n*-alkane concentrations (Fig. 2a), even *n*-fatty acids concentrations (Fig. 2b) and even *n*-alkanols concentrations (Fig. 2c) increased down core and were highest in Unit 3. The CPI<sub>25.33</sub> of *n*-alkanes ranged from 0.4 to 7.8 (avg. 3.9 ± 1.7; Fig. 2d) and the SC:LC ratio, from 0.2 to 3.3 (Fig. 3b) within the icy permafrost, with little difference between unit 2 and 3. The dominant *n*-alkane was C<sub>18</sub> in Unit 2 (except for a dominance of C<sub>27</sub> at the ice table), whereas Unit 3 was dominated by C<sub>25</sub> (Fig. 2D). The sum of the concentrations of hopanoids decreased within the icy permafrost, averaging 59.5 ± 58.9 μg g<sup>-1</sup> TOC in Unit 2 and 25.9 ± 18.0 μg g<sup>-1</sup> TOC in Unit 3 (Fig. 3D). Phytane (Pr), pristane (Ph) and phytol were also detected in highest concentrations in Unit 3 (Fig. 3D). Pr.Ph ratios ranged from 0.2 to 2.2 in the icy permafrost and decreased with depth (Fig. 3c).

Deleted: 2d

Deleted: 2c

Deleted: 3

Deleted: 4a

Deleted: 5a

Deleted: 3b

Deleted: c

Deleted: 3e

Deleted: 6

Deleted: 6c

Deleted: / Deleted: 6d

**Deleted:** Overall, these indices display a gradient of organic carbon degradation that decreases downcore through the icy permafrost. The hierarchal clustering analysis suggest higher level of organic carbon degradation in the dry permafrost, intermediate level in unit 2 and lower level in unit 3.

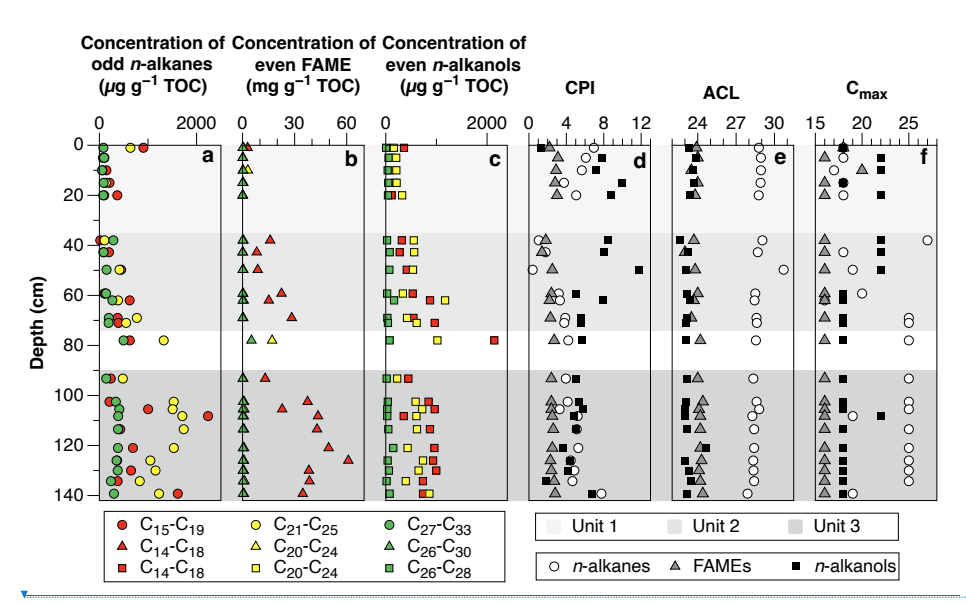
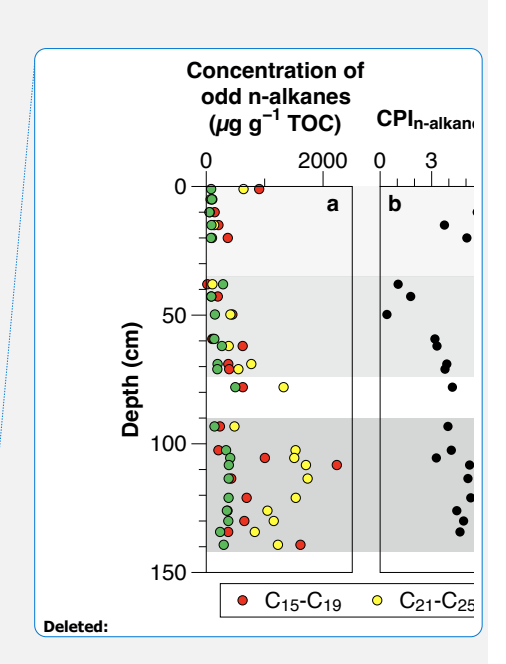


Figure 2 General distribution of biomarkers in core FHDP2C. a. concentration per gram organic carbon of low-molecular weight odd *n*-alkanes (*n*-C<sub>15</sub> to *n*-C<sub>19</sub>), mid molecular weight odd *n*-alkanes (*n*-C<sub>27</sub> to *n*-C<sub>25</sub>) and high-molecular weight odd *n*-alkanes (*n*-C<sub>27</sub> to *n*-C<sub>33</sub>), b. concentration per gram organic carbon of even low-molecular weight FAME (*n*-C<sub>14</sub> to *n*-C<sub>18</sub>), even mid molecular weight FAME (*n*-C<sub>20</sub> to *n*-C<sub>20</sub>) and even high-molecular weight FAME (*n*-C<sub>20</sub> to *n*-C<sub>20</sub>), c. concentration per gram organic carbon of even low-molecular weight *n*-alkanols (*n*-C<sub>14</sub> to *n*-C<sub>18</sub>), even mid-molecular weight *n*-alkanols (*n*-C<sub>24</sub>, and even high-molecular weight *n*-alkanols (*n*-C<sub>26</sub> to *n*-C<sub>28</sub>), d. carbon preference index (CPI) of *p*-alkanes (*n*-C<sub>25</sub> to *n*-C<sub>33</sub>), FAME (*n*-C<sub>22</sub> to *n*-C<sub>28</sub>), and *n*-alkanols (*n*-C<sub>27</sub> to *n*-C<sub>28</sub>), even mid-molecular weight *n*-alkanes (*n*-C<sub>27</sub> to *n*-C<sub>33</sub>), FAME (*n*-C<sub>22</sub> to *n*-C<sub>33</sub>), and *n*-alkanols (*n*-C<sub>22</sub> to *n*-C<sub>28</sub>), and, f. dominant *n*-alkane, FAME and *p*-alkanol (chain length).

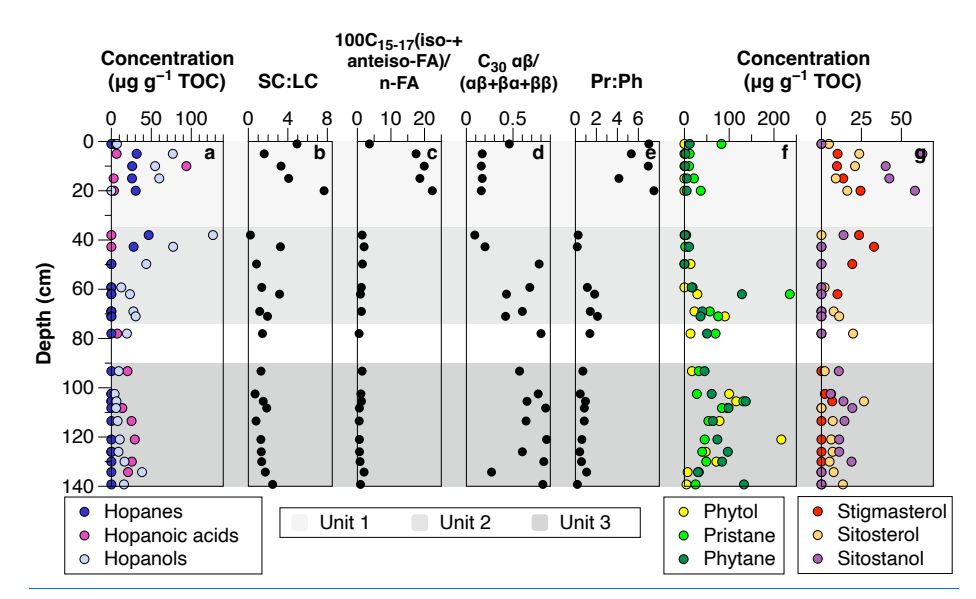
520



Formatted: Font: 9 pt, Italic

Moved (insertion) [4]
Formatted: Font: 9 pt, Italic

Formatted: Don't keep with next



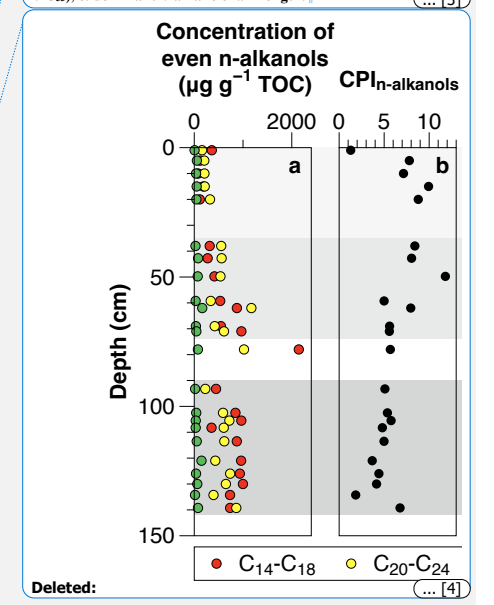
525 Figure 3 Diagnostic biomarker indices to differentiate between bacteria-derived and plant-derived organic matter. a. hopanes, hopanoic acids and hopanols, b. SC/LC (short-chain/long-chain) ratio of n-alkanes, c. ratio of iso-+anteiso- to straight chain FAME (n-C<sub>15</sub> to n-C<sub>17</sub>), d. C<sub>30</sub> αβ/(αβ+βα+ββ) hopane index, e. pristane/phytane ratio (Pr:Ph ratio), f. phytol, pristane and phytane and g. plant sterols.

Formatted: Caption, Don't keep with next

Formatted: Font: Italic

Moved up [4]: dominant n-alkane chain length.

Deleted: Figure 3 *n*-Alkane parameters of the Friis Hills drill core. a. concentration per gram organic carbon of low molecular weight odd *n*-alkanes (*n*-C<sub>15</sub> to *n*-C<sub>15</sub>), mid molecular weight odd *n*-alkanes (*n*-C<sub>21</sub> to *n*-C<sub>25</sub>) and high molecular weight odd *n*-alkanes (*n*-C<sub>27</sub> to *n*-C<sub>35</sub>), b. carbon preference index (CPI; *n*-C<sub>25</sub> to *n*-C<sub>35</sub>), c. SC/LC (short-chain/long-chain) ratio, d. average chain length (ACL) for high molecular weight *n*-alkanes (*n*-C<sub>27</sub> to *n*-C<sub>35</sub>), e. dominant *n*-alkane chain length.



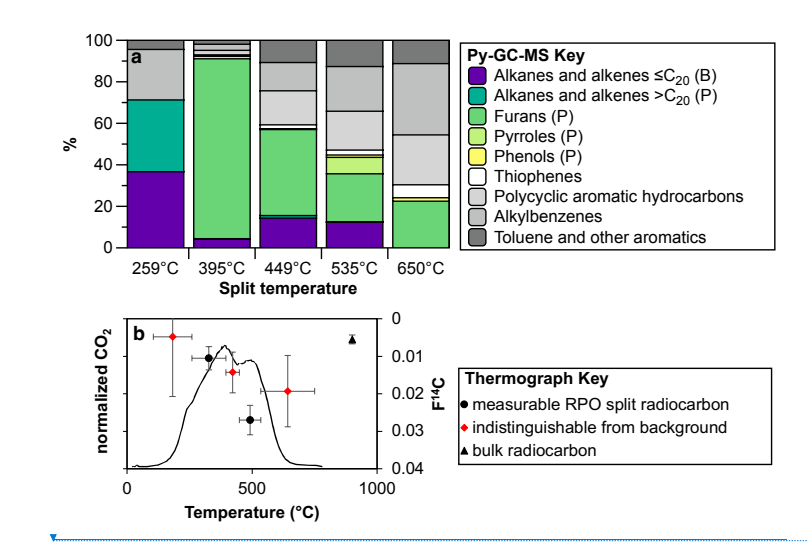


Figure 4 Py-GC MS split composition for sample 2-C0-3, situated at 10 cm depth in the dry permafrost layer, a. compounds are classified approximately on bacterial- (B) or plant- (P) derived sources based on carbon number of alkanes and alkenes detected. b. RPO thermograph of CO<sub>2</sub> evolution and RPO and bulk radiocarbon measurements. Note: data points in red are indistinguishable from background measurements.

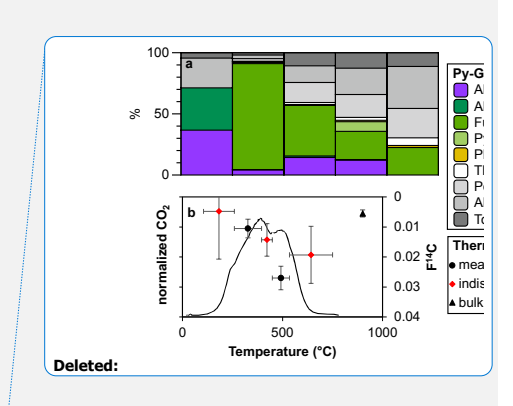
### 5 Discussion

### 5.1 Content and source of organic carbon: the legacy of the mid-Miocene tundra ecosystem

Soil organic carbon density in the dry and icy permafrost 140 cm core from Friis hills is about 4 times higher than those found in other ultraxerous soils like University Valley (SFig. 2; Faucher et al., 2017) and soils in the Mackay Glacier region (Van Goethem et al., 2020), but multiple orders of magnitude less than carbon stocks in mineral soils of maritime Antarctica (e.g. Alekseev and Abakumov, 2024; Simas et al., 2007). Currently, no vascular plants grow in the MDV (e.g. Virginia and Wall, 1999). As such, the low SOCd in most Quaternary-age soils in the MDV is attributed to the soil organic carbon being sourced either from endolithic micro-organisms (Faucher et al., 2017), glacially eroded material from older Cenozoic sediment and/or the Beacon Sandstone (e.g. Matsumoto et al., 1990a, Matsumoto et al., 2010), or Holocene age legacy carbon from aquatic systems (e.g. Lancaster, 2002, Barrett et al., 2006).

Conversely, the higher SOCd at Friis Hills is attributed to the tundra ecosystem that occupied the site during the mid-Miocene.

The tundra macrofossil assemblage from the site included lichens, liverworts, mosses, dicots, grasses and sedges, along with



Formatted: Caption, Don't keep with next

Deleted: Figure 7 Py-GC MS split composition for sample 2-C0-3, situated at 10 cm depth in the dry permafrost layer. a. compounds are classified approximately on bacterial- (B) or plant- (P) derived sources based on carbon number of alkanes and alkenes detected. b. RPO thermograph of CO<sub>2</sub> evolution and RPO and bulk radiocarbon measurements. Note: data points in red are indistinguishable from background measurements.

cuticles belonging to the *Nothofagaceae* family (Chorley et al., 2023). The lipid biomarkers that had a homogenous distribution in the 140 cm core are also consistent with the macrofossils assemblage. The BIT index of 1.0 derived from the brGDGTs samples suggests a fully terrestrial environment. The presence of high molecular weight *n*-alkanes, *n*-fatty acids and *n*-alkanols, along with phytosterols (i.e. sitosterol, stigmasterol and their respective stanols) and phytol (and pristane/phytane) are all indicative of a terrestrial environment dominated by higher order plants (Kögel-Knabner and Amelung, 2014; and references therein). The presence of mid-molecular weight (C<sub>21</sub>-C<sub>25</sub>) *n*-alkanes, *n*-fatty acids and *n*-alkanols indicate contributions of mosses and lichens. Thus, the Friis Hills sediments harbour a tundra-type biomarker signature and explains why Friis Hills has higher SOCd than other sites in the MDV (Fig. S3).

Deleted: 2

### 5.2 Degradation of organic carbon in the dry permafrost

595

620

The hierarchal clustering analysis of the samples in the 1.4 m core produced three groups and the variables and indices that were statistically different between the units. The dry permafrost (0-35cm) experienced a <u>relatively higher</u> degree of organic carbon degradation by microbes, whereas the underlying icy permafrost (38-71cm) experienced <u>relatively lower Jevels</u> of degradation.

The dry permafrost had C:N ratios near the Redfield ratio (Fig. 1c), higher δ<sup>13</sup>Corg (Fig. 1d), a higher proportion of iso- and anteiso-FAs relative to *n*-FAs (Fig. 3c), low phytol (Fig. 3f), high Pr:Ph (Fig. 3e), low C<sub>30</sub> αβ/(αβ+βα+ββ) hopane index (Fig. 3d), and a higher contributions of low-molecular weight homologues of *n*-alkanes (Fig. 3h). All of these indicators can be attributed to a balanced microbial activity that degraded the ancient organic carbon in Unit 1. The relative higher concentration of phytosterols, pristane, phytane and phytol in the dry permafrost (Fig. 3f) & g), the dominance of hopanoids (Fig. 3g) and the absence of steranes, compounds that possess similar long-term preservation potential (Love and Zumberge, 2021), can all be attributed to the higher degradation of the plant material (Fig. 5). Moreover, the Py-GC-MS measurements in the thermally partitioned splits for a sample in the dry permafrost indicate a high level of refractory organic matter and degraded organic carbon.

Active microbial growth in dry permafrost has also been reported in other ultraxerous soils. For example, in University Valley, the soils that experience temperature above 0°C and where the icy permafrost is recharged by snowmelt, the C:N ratios were also distributed along the Redfield ratio (Fig. S2; Faucher et al., 2017). Similar ratios were found in the Mackay Glacier region of East Antarctica, supporting active nutrient cycling, although low respiration rates were associated with dormancy (Van Goethem et al., 2020). At Friis Hills, the ice table and underlying icy permafrost is being recharged by evaporated snowmelt (Verret et al., 2022). As such the dry permafrost transiently receives input of liquid water that could support microbial activity, similar to the endoliths growing in bedrocks (e.g. Friedmann, 1982), and to the water tracks that form in spring and summer (Chan-Yam et al., 2019). <sup>14</sup>C of bulk sample indicate active microbial activity is small (<1%; using a simple two-component mixing model and assuming F<sub>1</sub><sup>14</sup>C=0.5 for Holocene carbon, with a half-life of 5.730 yrs), but yet it is producing degradation of organic carbon over large time-scales (as shown in the biomarker results). As such, microbial activity is occurring at very

Deleted: intermediate

Deleted: 2d

Deleted: 2c

Deleted: 4

Deleted: 6c

Deleted: c

Deleted: 6

Deleted: s

Deleted: c & 6c

Formatted: Superscript

low rates, only when sufficient moisture is present in the dry permafrost layer. The rest of the time, the soil ecosystem appears to remain mostly dormant (e.g. Van Goethem et al., 2020).

Deleted: enough

Deleted: s

### 640 5.3 Degradation of organic carbon in the icy permafrost

destabilized during past warm periods in the near surface.

650

The degradation of organic carbon is not limited to the dry permafrost and it can also be observed in the underlying icy permafrost (unit 2: 38-71cm). Units 1 and 2 both display a higher concentration of hopanoids and higher SC:LC ratios than Unit 3 (Fig. 3). Additionally,  $\delta^{13}C_{org}$  values show a sharp shift below the ice table, and between Unit 2 and 3, where the average  $\delta^{13}C_{org}$  changes from -25.2 ± 0.7% to -21.4 ± 1.4% VPDB (Fig. 1d). This shift in  $\delta^{13}C_{org}$  values suggests preferential loss of

<sup>12</sup>C in CO<sub>2</sub> from respiration and organic matter degradation, which leads to sediment enriched in δ<sup>13</sup>C<sub>org</sub>. The samples just below the ice table also have the lowest CPI<sub>n-alkane</sub> and CPI<sub>FAME</sub> (Fig. 2d), showing a higher degree of degradation.

These findings imply that rates of microbial organic matter degradation dominated over primary production of organic matter

at a point in time following the mid-Miocene climate transition, which could not be precisely dated. The original biomarker signatures would have been preserved throughout the sediment column if the upper part of the permafrost column had remained permanently frozen until present day, preventing extensive bacterial degradation. However, recognizing the increased degradation state of plant-derived organic matter and higher contributions from bacterial lipids in the shallower part of the record suggests overprint of the original lipid distribution during more recent periods when the active layer thawed to that depth. Based on a study on <sup>10</sup>Be<sub>met</sub> concentrations in the upper section of the FHDP2C core, the onset of hyper-arid conditions occurred around 6.0 Ma (Verret et al., 2023); although it is uncertain if continuous or intermittent wet conditions prevailed throughout the late Miocene period and ended at 6.0 Ma, Either way, before 6.0 Ma, an active layer that seasonally thawed was present in at the Friis Hills, which could explain the higher degradability of Unit 2 compared to Unit 3. The transition from Unit 2 to 3 at ~80 cm depth could therefore represent the position of a paleo layer of increased biological activity within a relict active layer. Similar trends have been observed the in the Arctic, where paleo-active layers are identified biogeochemically by a higher degree of degradation. (e.g. Lacelle et al., 2019). Furthermore, permafrost carbon reservoirs have also been destabilized at a large scale in the Arctic during past warm periods of the Pleistocene-Holocene (e.g. Tesi et

al., 2016). We show here that ancient permafrost carbon stocks in Antarctica, although marginal, could have also been

Deleted: s

Deleted: 8d

Deleted: 2c

Deleted: s 2c & 3c

**Deleted:** bacterial activity extended below the current ice table after the mid-Miocene

**Deleted:** or if a single warm period punctuated the late Miocene cooling trend at 6.0 Ma

Deleted: the

Deleted:

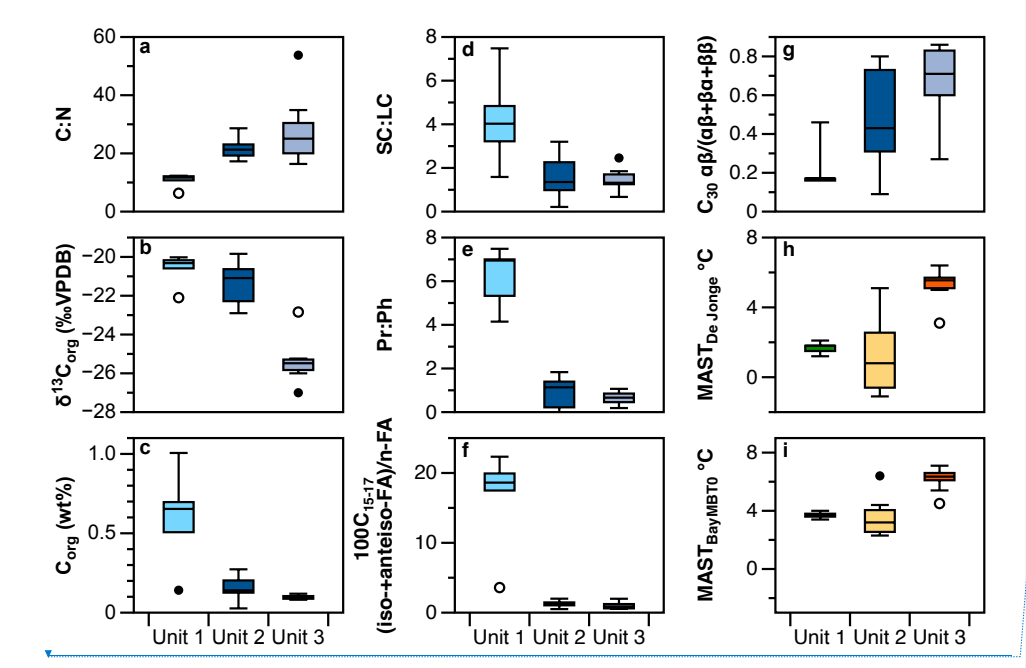
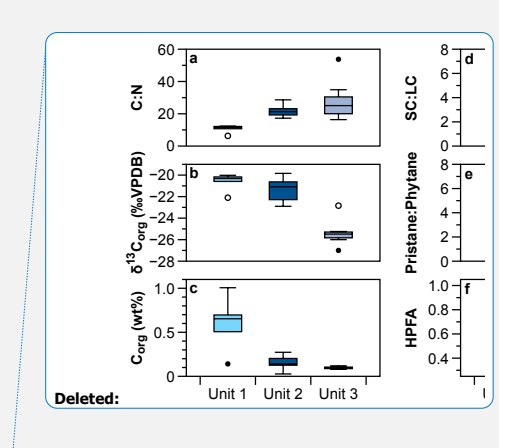


Figure 5 Boxplots of a. C:N ratio, b.  $\delta^{13}$ C, c. organic carbon, expressed in wt%, d. short-chain/long-chain n-alkane ratio, e. pristane/phytane ratio, f. ratio of iso-+anteiso- to straight chain FAME (n-C<sub>15</sub> to n-C<sub>17</sub>), g.  $C_{30}$   $\alpha\beta/(\alpha\beta+\beta\alpha+\beta\beta)$  hopane index and h-i. brGDGT ground temperature reconstructions for different units in core FHDP2C. These represent threshold temperatures for unlocking organic matter at different depths in the core: Unit 1 (0-35 cm depth), Unit 2 (38 -71 cm depth) and Unit 3 (93-140 cm depth). Units are based on hierarchical clustering.

# $5.4\ Temperature\ thresholds\ to\ reactivate\ biological\ activity\ in\ the\ dry\ permafrost\ and\ paleo-active\ layer$

brGDGTs have been increasingly used to reconstruct past temperatures in Arctic permafrost because the methylation and cyclisation of brGDGTs can be correlated to ground surface temperature (e.g. Raberg et al., 2024). Previous studies in permafrost regions have made the assumption that microbial communities stored in permafrost reflect the environmental conditions at time of enclosement, not the current conditions (closed-system assumption; Kusch et al., 2019). However, this assumption does not take into account subsequent warm periods (which would result in a re-opening of the system). Therefore, the temperature reconstructions could correspond to either: (1) the temperature at time of enclosement (here the mid-Miocene) or (2) the temperature at time when the active layer last thawed to that depth and thus the threshold temperature to activate



#### Deleted:

Figure 8 Boxplot of a. C:N ratio, b.  $\delta^{13}$ C, c. organic carbon, expressed in wt%, d. short-chain/long-chain n-alkane ratio, e. pristane/phytane ratio and f. HPFA index. Units are based on hierarchical clustering.

Deleted:

bacteria activity at a given depth. Since the previous sections have shown clear signs of overprinting in units 1 and 2, and to some extent in unit 3, the latter assumption is more likely. Moreover, recent studies have shown that in cold regions, the brGDGT calibrations best represents the summer ground temperature, and not the mean air temperatures for which brGDGT results are typically calibrated (e.g. Raberg et al., 2024). However, in the ultraxerous zone of the MDV, the mean annual air temperatures approximates those at the ground surface temperatures since there is no vegetation, minimal snow cover and little organic material (Lacelle et al., 2016).

While soil calibrations for Antarctic sites are lacking, sites from Arctic permafrost in Svalbard, Greenland and Alaska are found in the global soil sample database of De Jonge et al. (2014) and these regions show the same dominance of pentamethylated and hexamethylated brGDGTs (Kusch et al., 2019). The BayMBT<sub>0</sub> calibration (Crampton-Flood et al., 2020) also offers a separate calibration that assumes brGDGT distributions only reflect months with mean air temperatures above freezing and was applied to the Antarctic Peninsula (Tibbett et al., 2022). We therefore used these two calibrations to reconstruct mean summer ground temperatures. Based on the conclusions from the previous sections, we attribute these temperatures in units 1 and 2 to be the threshold temperatures required to activate bacteria activity at different depths in core FHDP2C (November to February in the MDV; Obryk et al., 2020), while the minimal overprinting of biomarker signature in unit 3 likely represents conditions during the mid-Miocene. The distribution of all samples in core FHDP2C was dominated by brGDGTs. All samples had a BIT index of 1.0. MBT'5<sub>ME</sub> index ranged between 0.24 and 0.48 (Supplementary Data). We obtained temperatures varying between 2.3 and 7.1°C using the BayMBT<sub>0</sub> calibration (Crampton-Flood et al., 2020) and between -1.1 and 6.4°C using the De Jonge et al. (2014) calibration. The BayMBT<sub>0</sub> calibration yields slightly warmer (~1°C overall) temperature reconstruction than the DeJonge calibration (Figs. 5h & i). The dry permafrost layer would require a mean summer soil temperature of ~2-4°C to reactivate biological processes. The temperature required to unlock the organic matter, stored below the ice table seems a bit more uncertain but lies between 0°C near the ice table up to ~7°C down at 0.70 m (Figs 5h & i). The latter is in line with the mean summer air temperatures required to thaw the maximum active layer depth (based on meteoric Berylllium-10 concentrations) during the late Miocene (i.e. 7-10°C to thaw a maximum active layer depth of 2.74 m; Verret et al., 2023). In general, the temperature required to reactivate biological activity increases with depth since the thickness of the active layer is largely controlled by summer air temperature. The increase in threshold temperature to ~0°C near the ice table based on the De Jonge et al. (2014) calibration could be explained by the soil fauna having a high response rate to increased soil moisture (thawing ground ice) in the MDV (Niederberger et al., 2019; Andriuzzi et al., 2018). These temperature thresholds are in line with current conditions in the lower elevations of Taylor Valley at a site near Lake Fryxell (77°36'06.1"S, 163°08'19.6"E, 21 m a.s.l.; Bakermans et al., 2014), where the mean summer ground temperature is +2°C and psychrophilic species have the ability to function. In. short, the organic matter, in unit 3 has a low probability of being reactivated, while the section closest to the ice table, unit 2, has a much higher probability and hence is showing higher levels

Deleted: to

Deleted: estimate

Deleted: , but overall they show similar trends

Deleted: 9

Deleted: OM

Deleted: 1

Deleted: 4

Deleted: 0

Deleted: c

Deleted:

Deleted: OM

Deleted: t

725

of degradation.

### 6 Conclusions

Although our study suggests that Holocene organic carbon is being introduced at high elevation sites such as the Friis Hills, modern  $C_{org}$  contributions remain very low (<1%). Beyond the dry permafrost,  $C_{org}$  is dominantly ancient and highly degraded. Based on the ramped pyrolysis approach to characterise and date different carbon pools, it seems like soil ecosystems in the high elevations (>1000 m a.s.l) of the MDV rely mostly on exogenous sources of Core, in this case legacy carbon from the Miocene tundra environment, but could have also marginally been able fix carbon in situ through the Holocene. More detailed 750 radiocarbon studies should be conducted to prove the latter. Moreover, based on our biomarker findings suggesting a gradient of Corg degradation through the soil profile, we conclude that legacy carbon locked-in at depth in the permafrost has been bioavailable under past warmer climate post-deposition. Seasonal thawing during warm periods is at the origin of Corg degradation at depth. Such periods seem to be marginal over the last 14 Myrs. Carbon in the dry upper 35 cm of the core could be bioavailable at a mean ground summer temperature of +2°C, conditions similar to those found in the lower elevations of Taylor Valley. Carbon is a key physicochemical factor in the development of soil microbial communities (e.g. Cary et al., 2010). Therefore, future climate warming could lead to unlocking legacy sources of carbon which would cause considerable impacts on the structure and function of ecosystems in the MDV. Overall, the organic matter in the core appears to be compatible with a highly degraded signature of the mid-Miocene paleoenvironment, but also displays a gradual environmental over-print attributable to post-depositional conditions that is more important near the surface. This finding suggests that the organic matter enclosed within the permafrost at Friis Hills is stable and bacterial alteration is mostly inhibited. However, bacterial degradation has occurred during warmer periods: episodically down to 80 cm and potentially beyond 140 cm during the late Miocene and down to 35 cm through to Holocene.

# Data availability

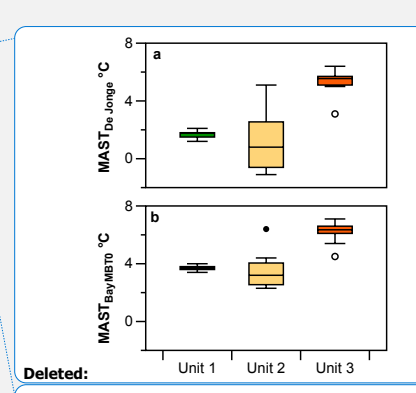
765 The data is uploaded as supplementary material.

### **Author Contributions**

M.V., S.N., D.L., W.D. and K.N. designed this project and contributed to data analysis/interpretation and writing the manuscript. M.V. and S.N. undertook the lipid biomarker analyses, C.G. and J.T. provided the ramped pyrolysis oxidation and radiocarbon analyses, whereas S.N. analysed and interpreted the Py-GC-MS data, R.L. developed the Friis Hills Drilling Project. All authors edited the whole manuscript.

### Competing interests

One of the co-authors of this manuscript is a member of the editorial board of Biogeosciences.



Deleted: Figure 9 brGDGT ground temperature reconstructions for different units in core FHDP2C. These represent threshold temperatures for unlocking OM at different depths in the core: Unit 1 (0-35 cm depth), Unit 2 (38 -71 cm depth) and Unit 3 (93-140 cm depth).

Deleted: OM

Deleted: ran

Deleted: experiment

Deleted: set

#### Acknowledgements

awarded to M. Verret in 2021. The Friis Hills Drilling Project (austral summer 2016–2017) was funded by the New Zealand Ministry of Business, Innovation and Employment through the Past Antarctic Science Programme (C05X1001) and the Antarctic Science Platform (ANTA1801) to R. Levy and T. Naish. We acknowledge Strategic Science Investment Funding (SSIF) from the New Zealand Ministry of Business, Innovation and Employment as part of the Global Change Through Time Programme (contract C05X1702). We thank A. Pyne, R. Pyne, H. Chorley and Webster Drilling for retrieving the cores at

This work was funded by the New Zealand Antarctic Research Institute through an Early Career Researcher Seed Grant

cores. Laboratory work was made possible with the help of the technical staff at the Sedimentology and Water Quality Laboratory at the Victoria University of Wellington (J. Chewings), the Geography Laboratory at the University of Ottawa (J. Bjornson), the Ján Veizer Stable Isotope Laboratory (P. Middlestead, W. Abdi and P. Wickham) and the Rafter Radiocarbon Laboratory, GNS Science New Zealand (J. Dahl and T. Ferrick).

Friis Hills. A special thank you to N. Bertler for allowing us to use the GNS Ice Core Facility to store and sample the permafrost

### References

Alekseev, I. and Abakumov, E.: Soil organic matter and biogenic-abiogenic interactions in soils of Larsemann Hills and Bunger
Hills, East Antarctica, Polar Science, 40, 101040, https://doi.org/10.1016/j.polar.2023.101040, 2024.

Allibone, A. H., Cox, S. C., Graham, I. J., Smellie, R. W., Johnstone, R. D., Ellery, S. G., and Palmer, K.: Granitoids of the

Allibone, A. H., Cox, S. C., Graham, I. J., Smellie, R. W., Johnstone, R. D., Ellery, S. G., and Palmer, K.: Granitoids of the Dry Valleys area, southern Victoria Land, Antarctica: plutons, field relationships, and isotopic dating, New Zealand Journal of Geology and Geophysics, 36, 281-297, <a href="https://doi.org/10.1080/00288306.1993.9514576">https://doi.org/10.1080/00288306.1993.9514576</a>, 1993.

Andriuzzi, W., Adams, B., Barrett, J., Virginia, R., and Wall, D.: Observed trends of soil fauna in the Antarctic Dry Valleys:

early signs of shifts predicted under climate change, Ecology, 99, 312-321, <a href="https://doi.org/10.1002/ecy.2090">https://doi.org/10.1002/ecy.2090</a>, 2018. Bakermans, C., Skidmore, M. L., Douglas, S., and McKay, C. P.: Molecular characterization of bacteria from permafrost of the Taylor Valley, Antarctica, FEMS Microbiology Ecology, 89, 331-346, <a href="https://doi.org/10.1111/1574-6941.12310">https://doi.org/10.1111/1574-6941.12310</a>, 2014. Bargagli, R., Sanchez-Hernandez, J., and Monaci, F.: Baseline concentrations of elements in the Antarctic macrolichen

Umbilicaria decussata, Chemosphere, 38, 475-487, <a href="https://doi.org/10.1016/S0045-6535(98)00211-2">https://doi.org/10.1016/S0045-6535(98)00211-2</a>, 1999.
 Barrett, J. E., Virginia, R. A., Lyons, W. B., McKnight, D. M., Priscu, J. C., Doran, P. T., Fountain, A. G., Wall, D. H., and Moorhead, D.: Biogeochemical stoichiometry of Antarctic dry valley ecosystems, Journal of Geophysical Research: Biogeosciences, 112, <a href="https://doi.org/10.1029/2005JG000141">https://doi.org/10.1029/2005JG000141</a>, 2007.
 Berke, M. A., Sierra, A. C., Bush, R., Cheah, D., and O'Connor, K.: Controls on leaf wax fractionation and 8<sup>2</sup>H values in

tundra vascular plants from western Greenland, Geochimica et Cosmochimica Acta, 244, 565-583, <a href="https://doi.org/10.1016/j.gea.2018.10.020">https://doi.org/10.1016/j.gea.2018.10.020</a>, 2019.

Bliss, A. K., Cuffey, K. M., and Kavanaugh, J. L.: Sublimation and surface energy budget of Taylor Glacier, Antarctica, Journal of Glaciology, 57, 684-696, <a href="https://doi.org/10.3189/002214311797409767">https://doi.org/10.3189/002214311797409767</a>, 2011.

Bray, E. and Evans, E.: Distribution of *n*-paraffins as a clue to recognition of source beds, Geochimica et Cosmochimica Acta, 22, 2-15, <a href="https://doi.org/10.1016/0016-7037(61)90069-2">https://doi.org/10.1016/0016-7037(61)90069-2</a>, 1961.

820 Cary, S. C., McDonald, I. R., Barrett, J. E., and Cowan, D. A.: On the rocks: the microbiology of Antarctic Dry Valley soils, Nature Reviews Microbiology, 8, 129-138, <a href="https://doi.org/10.1038/nrmicro2281">https://doi.org/10.1038/nrmicro2281</a>, 2010.
Castañeda, I. S. and Schouten, S.: A review of molecular organic proxies for examining modern and ancient lacustrine environments, Quaternary Science Reviews, 30, 2851-2891, <a href="https://doi.org/10.1016/j.quascirev.2011.07.009">https://doi.org/10.1016/j.quascirev.2011.07.009</a>, 2011.

Chan-Yam, K., Goordial, J., Greer, C., Davila, A., McKay, C. P., and Whyte, L. G.: Microbial activity and habitability of an Antarctic dry valley water track, Astrobiology, 19, 757-770, https://doi.org/10.1089/ast.2018.1884, 2019.

### Moved (insertion) [1]

Moved up [1]: We acknowledge Strategic Science Investment Funding (SSIF) from the New Zealand Ministry of Business, Innovation and Employment as part of the Global Change Through Time Programme (contract C05X1702).

- 830 Chorley, H., Levy, R., Naish, T., Lewis, A., Cox, S., Hemming, S., Ohneiser, C., Gorman, A., Harper, M., Homes, A., Hopkins, J., Prebble, J., Verret, M., Dickinson, W., Florindo, F., Golledge, N., Halberstadt, A. R., Kowalewski, D., McKay, R., Meyers, S., Anderson, J., Dagg, B., and Lurcock, P.: East Antarctic Ice Sheet variability during the middle Miocene Climate Transition captured in drill cores from the Friis Hills, Transantarctic Mountains, GSA Bulletin, 135, 1503-1529, https://doi.org/10.1130/B36531.1, 2023.
- 835 Cox, S., Turnbull, I., Isaac, M., Townsend, D., and Lyttle, B.: Geology of southern Victoria Land, Antarctica, Institute of Geological & Nuclear Sciences 1:250 000 geological map 22. 1 sheet + 135 pp, GNS Science, Lower Hutt, New Zealand, 2012.
  - Crampton-Flood, E. D., Tierney, J. E., Peterse, F., Kirkels, F. M., and Damsté, J. S. S.: BayMBT: A Bayesian calibration model for branched glycerol dialkyl glycerol tetraethers in soils and peats, Geochimica et Cosmochimica Acta, 268, 142-159, https://doi.org/10.1016/j.gca.2019.09.043, 2020.
  - De Jonge, C., Hopmans, E. C., Zell, C. I., Kim, J.-H., Schouten, S., and Damsté, J. S. S.: Occurrence and abundance of 6-methyl branched glycerol dialkyl glycerol tetraethers in soils: Implications for palaeoclimate reconstruction, Geochimica et Cosmochimica Acta, 141, 97-112, <a href="https://doi.org/10.1016/j.gea.2014.06.013">https://doi.org/10.1016/j.gea.2014.06.013</a>, 2014.
  - Donahue, D. J., Linick, T. W., and Jull, A. T.: Isotope-ratio and background corrections for accelerator mass spectrometry radiocarbon measurements, Radiocarbon, 32, 135-142, https://doi.org/10.1017/S0033822200040121, 1990.
  - Doran, P. and Fountain, A.: McMurdo Dry Valleys Friis Hills Meteorological Station Monthly Averages [dataset], <a href="https://doi.org/10.6073/pasta/9b2adf7484d75b0ab66c2080c3fbe91b">https://doi.org/10.6073/pasta/9b2adf7484d75b0ab66c2080c3fbe91b</a>, 2016.
  - Dragone, N. B., Diaz, M. A., Hogg, I. D., Lyons, W. B., Jackson, W. A., Wall, D. H., Adams, B. J., and Fierer, N.: Exploring the boundaries of microbial habitability in soil, Journal of Geophysical Research: Biogeosciences, 126, e2020JG006052, https://doi.org/10.1029/2020JG006052, 2021.
  - Duncan, B., McKay, R., Bendle, J., Naish, T., Inglis, G. N., Moossen, H., Levy, R., Ventura, G. T., Lewis, A., and Chamberlain, B.: Lipid biomarker distributions in Oligocene and Miocene sediments from the Ross Sea region, Antarctica: Implications for use of biomarker proxies in glacially-influenced settings, Palaeogeography, Palaeoclimatology, Palaeoecology, 516, 71-89, https://doi.org/10.1016/j.palaeo.2018.11.028, 2019.
  - 5 Eigenbrode, J. L.: Fossil lipids for life-detection: a case study from the early Earth record, Space Science Reviews, 135, 161-185, https://doi.org/10.1007/s11214-007-9252-9, 2008.
    Farrimond, P., Taylor, A., and Telnæs, N.: Biomarker maturity parameters: the role of generation and thermal degradation, Organic Geochemistry, 29, 1181-1197, https://doi.org/10.1016/S0146-6380(98)00079-5, 1998.
  - Faucher, B., Lacelle, D., Davila, A., Pollard, W., Fisher, D., and McKay, C. P.: Physicochemical and biological controls on carbon and nitrogen in permafrost from an ultraxerous environment, McMurdo Dry Valleys of Antarctica, Journal of Geophysical Research: Biogeosciences, 122, 2593-2604, <a href="https://doi.org/10.1100/2/0017JG004006">https://doi.org/10.1100/2/0017JG004006</a>, 2017.
    Flower, B. P. and Kennett, J. P.: The middle Miocene climatic transition: East Antarctic ice sheet development, deep ocean circulation and global carbon cycling, Palaeogeography, palaeocclimatology, palaeoecology, 108, 537-555,
  - https://doi.org/10.1016/0031-0182(94)90251-8, 1994.

    Freckman, D. W. and Virginia, R. A.: Low-diversity Antarctic soil nematode communities: distribution and response to disturbance, Ecology, 78, 363-369, <a href="https://doi.org/10.1890/0012-9658(1997)078[0363:LDASNC]2.0.CO;2">https://doi.org/10.1890/0012-9658(1997)078[0363:LDASNC]2.0.CO;2</a>, 1997.

    Friedmann, E. I.: Endolithic microorganisms in the Antarctic cold desert, Science, 215, 1045-1053, https://lo.1126/science.215.4536.1045, 1982.
- Ginnane, C. E., Turnbull, J. C., Naeher, S., Rosenheim, B. E., Venturelli, R. A., Phillips, A. M., Reeve, S., Parry-Thompson,
   J., Zondervan, A., and Levy, R. H.: Advancing Antarctic sediment chronology through combined ramped pyrolysis oxidation and pyrolysis GC-MS, Radiocarbon, 66(5), 1120-1139, <a href="https://doi.org/10.1017/RDC.2023.116">https://doi.org/10.1017/RDC.2023.116</a>, 2024.
   Goordial, J., Davila, A., Lacelle, D., Pollard, W., Marinova, M. M., Greer, C. W., DiRuggiero, J., McKay, C. P., and Whyte,
   L. G.: Nearing the cold-arid limits of microbial life in permafrost of an upper dry valley, Antarctica, The ISME journal, 10, 1613-1624. 2016.
- 875 Haugk, C., Jongejans, L. L., Mangelsdorf, K., Fuchs, M., Ogneva, O., Palmtag, J., Mollenhauer, G., Mann, P. J., Overduin, P. P., and Grosse, G.: Organic matter characteristics of a rapidly eroding permafrost cliff in NE Siberia (Lena Delta, Laptev Sea region), Biogeosciences, 19, 2079-2094, https://doi.org/10.5194/bg-19-2079-2022, 2022.

- Hopkins, D., Sparrow, A., Gregorich, E., Elberling, B., Novis, P., Fraser, F., Scrimgeour, C., Dennis, P., Meier-Augenstein, W., and Greenfield, L.: Isotopic evidence for the provenance and turnover of organic carbon by soil microorganisms in the
- 880 Antarctic dry valleys, Environmental microbiology, 11, 597-608, <a href="https://doi.org/10.1111/j.1462-2920.2008.01830.x">https://doi.org/10.1111/j.1462-2920.2008.01830.x</a>, 2009. Hopmans, E. C., Schouten, S., and Damsté, J. S. S.: The effect of improved chromatography on GDGT-based palaeoproxies, Organic Geochemistry, 93, 1-6, <a href="https://doi.org/10.1016/j.orggeochem.2015.12.006">https://doi.org/10.1016/j.orggeochem.2015.12.006</a>, 2016.
  - Hopmans, E. C., Weijers, J. W., Schefuß, E., Herfort, L., Damsté, J. S. S., and Schouten, S.: A novel proxy for terrestrial organic matter in sediments based on branched and isoprenoid tetraether lipids, Earth and Planetary Science Letters, 224, 107-
- 885 116, https://doi.org/10.1016/j.epsl.2004.05.012, 2004.
  - Horowitz, N. H., Cameron, R. E., and Hubbard, J. S.: Microbiology of the Dry Valleys of Antarctica: Studies in the world's coldest and driest desert have implications for the Mars biological program, Science, 176, 242-245, https://10.1126/science.176.4032.242, 1972.
  - Juggins, S.: Package 'rioja': An R Package for the Analysis of Quaternary Science Data., 0.9 [code], 2020.
- 890 Kaal, J.: Analytical pyrolysis in marine environments revisited, Analytical Pyrolysis Letters, 6, 1-16, 2019.
  - Kaneda, T.: Iso-and anteiso-fatty acids in bacteria: biosynthesis, function, and taxonomic significance, Microbiological reviews, 55, 288-302, <a href="https://doi.org/10.1128/mr.55.2.288-302.1991">https://doi.org/10.1128/mr.55.2.288-302.1991</a>, 1991.
  - Keely, B. J.: Geochemistry of chlorophylls, in: Chlorophylls and bacteriochlorophylls: biochemistry, biophysics, functions and applications, Springer, 535-561, <a href="https://doi.org/10.1007/1-4020-4516-6\_37">https://doi.org/10.1007/1-4020-4516-6\_37</a>, 2006.
- Killops, S. and Killops, V.: Introduction to Organic Geochemistry, 2nd edition, John Wiley & Sons; , 408 pages pp.2013. Kögel-Knabner, I. and Amelung, W.: 12.7 Dynamics, Chemistry, and Preservation of Organic Matter in Soils, in: Treatise on Geochemistry (Second Edition), edited by: Holland, H. D., and Turekian, K. K., Elsevier, 157-215, <a href="https://doi.org/10.1016/B978-0-08-095975-7.01012-3">https://doi.org/10.1016/B978-0-08-095975-7.01012-3</a>, 2014.
- Kusch, S., Rethemeyer, J., Ransby, D., and Mollenhauer, G.: Permafrost organic carbon turnover and export into a high-Arctic fjord: A case study from Svalbard using compound-specific <sup>14</sup>C analysis, Journal of Geophysical Research: Biogeosciences, 126, e2020JG006008, <a href="https://doi.org/10.1029/2020JG006008">https://doi.org/10.1029/2020JG006008</a>, 2021.

  Kusch, S., Winterfeld, M., Mollenhauer, G., Höfle, S. T., Schirrmeister, L., Schwamborn, G., and Rethemeyer, J.: Glycerol
  - dialkyl glycerol tetraethers (GDGTs) in high latitude Siberian permafrost: Diversity, environmental controls, and implications for proxy applications, Organic Geochemistry, 136, 103888, <a href="https://doi.org/10.1016/j.orgeochem.2019.06.009">https://doi.org/10.1016/j.orgeochem.2019.06.009</a>, 2019. Lacelle, D., Fontaine, M., Pellerin, A., Kokelj, S. V., and Clark, I. D.: Legacy of holocene landscape changes on soil biogeochemistry: a perspective from paleo-active lavers in Northwestern Canada. Journal of Geophysical Research:
- Biogeosciences, 124, 2662-2679, https://doi.org/10.1029/2018JG004916, 2019.

  Lacelle, D., Lapalme, C., Davila, A. F., Pollard, W., Marinova, M., Heldmann, J., and McKay, C. P.: Solar radiation and air and ground temperature relations in the cold and hyper-arid Ouartermain Mountains. McMurdo Dry Valleys of Antarctica.
- 910 Permafrost and Periglacial Processes, 27, 163-176, <a href="https://doi.org/10.1002/ppp.1859">https://doi.org/10.1002/ppp.1859</a>, 2016.
  Lacelle, D., Davila, A. F., Fisher, D., Pollard, W. H., DeWitt, R., Heldmann, J., Marinova, M. M., and McKay, C. P.: Excess ground ice of condensation-diffusion origin in University Valley, Dry Valleys of Antarctica: Evidence from isotope geochemistry and numerical modeling, Geochimica et Cosmochimica Acta, 120, 280-297
- https://doi.org/10.1016/j.gca.2013.06.032, 2013.

  1915 Lawson, J., Doran, P. T., Kenig, F., Des Marais, D. J., and Priscu, J. C.: Stable carbon and nitrogen isotopic, Aquatic Geochemistry, 10, 269-301, https://doi.org/10.1007/s10498-004-2262-2, 2004.

  Lewis, A. R. and Ashworth, A. C.: An early to middle Miocene record of ice-sheet and landscape evolution from the Friis Hills, Antarctica, Bulletin, 128, 719-738, https://doi.org/10.1130/B31319.1, 2016.
- Lewis, A. R., Marchant, D. R., Ashworth, A. C., Hedenäs, L., Hemming, S. R., Johnson, J. V., Leng, M. J., Machlus, M. L.,
   Newton, A. E., and Raine, J. I.: Mid-Miocene cooling and the extinction of tundra in continental Antarctica, Proceedings of the National Academy of Sciences, 105, 10676-10680, <a href="https://doi.org/10.1073/pnas.0802501105">https://doi.org/10.1073/pnas.0802501105</a>, 2008.
   Love, G. D. and Zumberge, J. A.: Emerging patterns in proterozoic lipid biomarker records, Elements in Geochemical Tracers in Earth System Science, Cambridge University Press, <a href="https://doi.org/10.1017/9781108847117">https://doi.org/10.1017/9781108847117</a>, 2021.
- Marchant, D. R. and Head III, J. W.: Antarctic dry valleys: Microclimate zonation, variable geomorphic processes, and
   implications for assessing climate change on Mars, Icarus, 192, 187-222, <a href="https://doi.org/10.1016/j.icarus.2007.06.018">https://doi.org/10.1016/j.icarus.2007.06.018</a>, 2007.
   Meyers, P. A.: Preservation of elemental and isotopic source identification of sedimentary organic matter, Chemical geology, 114, 289-302, <a href="https://doi.org/10.1016/0009-2541(94)90059-0">https://doi.org/10.1016/0009-2541(94)90059-0</a>, 1994.

- Meyers, P. A. and Ishiwatari, R.: Lacustrine organic geochemistry—an overview of indicators of organic matter sources and diagenesis in lake sediments, Organic geochemistry, 20, 867-900, https://doi.org/10.1016/0146-6380(93)90100-P, 1993.
- 930 Moorhead, D. L., Wall, D. H., Virginia, R. A., and Parsons, A. N.: Distribution and life-cycle of *Scottnema lindsayae* (Nematoda) in Antarctic soils: a modeling analysis of temperature responses, Polar Biology, 25, 118-125, https://doi.org/10.1007/s003000100319, 2002.
  - Naafs, B., Inglis, G., Blewett, J., McClymont, E. L., Lauretano, V., Xie, S., Evershed, R., and Pancost, R.: The potential of biomarker proxies to trace climate, vegetation, and biogeochemical processes in peat: A review, Global and Planetary Change,
- 935 179, 57-79, <a href="https://doi.org/10.1016/j.gloplacha.2019.05.006">https://doi.org/10.1016/j.gloplacha.2019.05.006</a>, 2019.

  Naeher, S. and Grice, K.: Novel 1H-Pyrrole-2, 5-dione (maleimide) proxies for the assessment of photic zone euxinia, Chemical Geology, 404, 100-109, <a href="https://doi.org/10.1016/j.chemgeo.2015.03.020">https://doi.org/10.1016/j.chemgeo.2015.03.020</a>, 2015.

- Naeher, S., Cui, X., and Summons, R. E.: Biomarkers: molecular tools to study life, environment, and climate, Elements: An International Magazine of Mineralogy, Geochemistry, and Petrology, 18, 79-85, <a href="https://doi.org/10.2138/gselements.18.2.79">https://doi.org/10.2138/gselements.18.2.79</a>, 2022
- Naeher, S., Niemann, H., Peterse, F., Smittenberg, R. H., Zigah, P. K., and Schubert, C. J.: Tracing the methane cycle with lipid biomarkers in Lake Rotsee (Switzerland), Organic Geochemistry, 66, 174-181, <a href="https://doi.org/10.1016/j.orggeochem.2013.11.002">https://doi.org/10.1016/j.orggeochem.2013.11.002</a>, 2014.
- Naeher, S., Smittenberg, R. H., Gilli, A., Kirilova, E. P., Lotter, A. F., and Schubert, C. J.: Impact of recent lake eutrophication on microbial community changes as revealed by high resolution lipid biomarkers in Rotsee (Switzerland), Organic Geochemistry, 49, 86-95, 2012.
  - Niederberger, T. D., Bottos, E. M., Sohm, J. A., Gunderson, T., Parker, A., Coyne, K. J., Capone, D. G., Carpenter, E. J., and Cary, S. C.: Rapid microbial dynamics in response to an induced wetting event in Antarctic Dry Valley soils, Frontiers in Microbiology, 10, 621, https://doi.org/10.3389/fmicb.2019.00621, 2019.
- 950 Obryk, M. K., Doran, P. T., Fountain, A. G., Myers, M., and McKay, C. P.: Climate from the McMurdo Dry Valleys, Antarctica, 1986–2017: surface air temperature trends and redefined summer season, Journal of Geophysical Research: Atmospheres, 125, e2019JD032180, <a href="https://doi.org/10.1029/2019JD032180">https://doi.org/10.1029/2019JD032180</a>, <a href="https://doi.org/10.1029/2019JD032180">https://doi.org/10.1029/2019JD032180</a>
  - Osburn, C. L., Anderson, N. J., Leng, M. J., Barry, C. D., and Whiteford, E. J.: Stable isotopes reveal independent carbon pools across an Arctic hydro-climatic gradient: Implications for the fate of carbon in warmer and drier conditions, Limnology and Oceanography Letters, 4, 205-213, <a href="https://doi.org/10.1002/lol2.10119">https://doi.org/10.1002/lol2.10119</a>, 2019.
    - Peters, K., Walters, C., and Moldowan, J.: Origin and preservation of organic matter, in: The biomarker guide Volume 1, 3-17, https://doi.org/10.1017/CBO9780511524868, 2004a.
    - Peters, K. E., Walters, C. C., and Moldowan, J. M.: Part II: Biomarkers and isotopes in petroleum systems and earth history, in: The biomarker guide Volume 2, Cambridge University Press, https://doi.org/10.1017/CBO9781107326040, 2004b.
- 960 Powell, T.: Pristane/phytane ratio as environmental indicator, Nature, 333, 604-604, <a href="https://doi.org/10.1038/333604a0">https://doi.org/10.1038/333604a0</a>, 1988.
  Poynter, J. and Eglinton, G.: 14. Molecular composition of three sediments from hole 717c: The Bengal fan, Proceedings of the Ocean Drilling Program: Scientific results, 155-161, <a href="https://10.2973/odp.proc.sr.116.151.1990">https://10.2973/odp.proc.sr.116.151.1990</a>,
  - Raberg, J. H., Crump, S. E., de Wet, G., Harning, D. J., Miller, G. H., Geirsdóttir, Á., and Sepúlveda, J.: BrGDGT lipids in cold regions reflect summer soil temperature and seasonal soil water chemistry, Geochimica et Cosmochimica Acta, https://doi.org/10.1016/j.gca.2024.01.034, 2024.
  - Redfield, A. C.: On the proportions of organic derivatives in sea water and their relation to the composition of plankton, university press of liverpool Liverpool 1934.
  - Reimer, P. J., Brown, T. A., and Reimer, R. W.: Discussion: reporting and calibration of post-bomb <sup>14</sup>C data, Radiocarbon, 46, 1299-1304, <a href="https://doi.org/10.1017/S0033822200033154">https://doi.org/10.1017/S0033822200033154</a>, 2004.
- 970 Schouten, S., Hopmans, E. C., and Damsté, J. S. S.: The organic geochemistry of glycerol dialkyl glycerol tetraether lipids: A review, Organic geochemistry, 54, 19-61, <a href="https://doi.org/10.1016/j.orggeochem.2012.09.006">https://doi.org/10.1016/j.orggeochem.2012.09.006</a>, 2013. Shevenell, A. E., Kennett, J. P., and Lea, D. W.: Middle Miocene southern ocean cooling and Antarctic cryosphere expansion, Science, 305, 1766-1770, <a href="https://lo.1126/science.1100061">https://lo.1126/science.1100061</a>, 2004.
- Simas, F., Schaefer, C., Mendonça, E., Silva, I., Santana, R., and Ribeiro, A.: Organic carbon stocks in permafrost-affected soils from Admiralty Bay, Antarctica, US Geological Survey and The National Academies, USGS OF-2007-1047, Short Research Paper, 76, https://10:3133/of2007-1047.srp076, 2007.

- Stuiver, M. and Polach, H. A.: Discussion reporting of 14C data, Radiocarbon, https://doi.org/10.1017/S0033822200003672, 1977.
- Tamppari, L., Anderson, R., Archer, P., Douglas, S., Kounaves, S., McKay, C., Ming, D., Moore, Q., Quinn, J., and Smith, P.: Effects of extreme cold and aridity on soils and habitability: McMurdo Dry Valleys as an analogue for the Mars Phoenix landing site, Antarctic Science, 24, 211-228, https://doi.org/10.1017/S0954102011000800, 2012.
  - Tesi, T., Muschitiello, F., Smittenberg, R. H., Jakobsson, M., Vonk, J., Hill, P., Andersson, A., Kirchner, N., Noormets, R., and Dudarey, O.: Massive remobilization of permafrost carbon during post-glacial warming, Nature Communications, 7, 13653, https://doi.org/10.1038/ncomms13653, 2016.
- Tibbett, E. J., Warny, S., Tierney, J. E., Wellner, J. S., and Feakins, S. J.: Cenozoic Antarctic Peninsula Temperatures and Glacial Erosion Signals From a Multi-Proxy Biomarker Study, Paleoceanography and Paleoclimatology, 37, e2022PA004430, https://doi.org/10.1029/2022PA004430, 2022.
- Turnbull, J. C., Zondervan, A., Kaiser, J., Norris, M., Dahl, J., Baisden, T., and Lehman, S.: High-precision atmospheric <sup>14</sup>CO<sub>2</sub> measurement at the Rafter Radiocarbon Laboratory, Radiocarbon, 57, 377-388, https://doi.org/10.2458/azu rc.57.18390, 990
  - Valletta, R. D., Willenbring, J. K., Lewis, A. R., Ashworth, A. C., and Caffee, M.: Extreme decay of meteoric beryllium-10 as a proxy for persistent aridity, Scientific reports, 5, 17813, https://doi.org/10.1038/srep17813, 2015.
  - Van Goethem, M. W., Vikram, S., Hopkins, D. W., Hall, G., Woodborne, S., Aspray, T. J., Hogg, I. D., Cowan, D. A., and Makhalanyane, T. P.: Nutrient parsimony shapes diversity and functionality in hyper-oligotrophic Antarctic soils, bioRxiv, https://doi.org/10.1101/2020.02.15.950717, 2020.
  - Verret, M., Dickinson, W., Lacelle, D., Fisher, D., Norton, K., Chorley, H., Levy, R., and Naish, T.: Cryostratigraphy of mid-Miocene permafrost at Friis Hills, McMurdo Dry Valleys of Antarctica, Antarctic Science, 33, 174-188, https://10.1017/S0954102020000619, 2021.
- Verret, M., Trinh-Le, C., Dickinson, W., Norton, K., Lacelle, D., Christl, M., Levy, R., and Naish, T.: Late Miocene onset of hyper-aridity in East Antarctica indicated by meteoric beryllium-10 in permafrost, Nature Geoscience, 1-7, https://doi.org/10.1038/s41561-023-01193-4, 2023.
  - Virginia, R. A. and Wall, D. H.: How soils structure communities in the Antarctic Dry Valleys, Bioscience, 49, 973-983, https://doi.org/10.1525/bisi.1999.49.12.973, 1999.
- Zech, M., Buggle, B., Leiber, K., Marković, S., Glaser, B., Hambach, U., Huwe, B., Stevens, T., Sümegi, P., and Wiesenberg, G.: Reconstructing Quaternary vegetation history in the Carpathian Basin, SE-Europe, using n-alkane biomarkers as molecular fossils: problems and possible solutions, potential and limitations, E&G Quaternary Science Journal, 58, 148-155, https://doi.org/10.3285/eg.58.2.03, 2010.
  - Zondervan, A., Hauser, T., Kaiser, J., Kitchen, R., Turnbull, J., and West, J.: XCAMS: The compact <sup>14</sup>C accelerator mass spectrometer extended for 10Be and 26Al at GNS Science, New Zealand, Nuclear Instruments and Methods in Physics Research
- Section B: Beam Interactions with Materials and Atoms, 361, 25-33, https://doi.org/10.1016/j.nimb.2015.03.013, 2015.

Formatted: Font: 10.5 pt, Not Italic

NZA #	RP Split	RP split min temp. (°C)	RP split max temp. (°C)	Split size (mg C)	CRA (yrs BP)	CRA Error	F <sup>14</sup> C	F <sup>14</sup> C Error	Comments
70400	Bulk			1.07	41,749	1,736	0.0055	0.0012	
75354	1	105	259	0.08	42,935	26,742	0.0048	0.0159	This sample is indistinguishable from the background measurements
75365	2	259	395	0.45	36,576	2,379	0.0105	0.0031	
75361	3	395	449	0.22	34,098	3,018	0.0143	0.0054	This sample is indistinguishabl from the background measurements
75364	4	449	535	0.32	29,004	1,158	0.0270	0.0039	
75359	5	535	750	0.17	31,716	3,971	0.0193	0.0095	This sample is indistinguishabl from the background measurements

Page 11: [1] Deleted	Marjolaine Verret	5/12/25 11:44:00 AM
Page 11: [2] Deleted	Marjolaine Verret	7/15/25 2:52:00 PM
V		
Page 14: [3] Deleted	Marjolaine Verret	7/15/25 2:49:00 PM
Page 14: [4] Deleted	Marjolaine Verret	5/8/25 11:45:00 AM
_		

l